

# On the evolution and fate of super-massive stars

L. R. Yungelson<sup>1,2,3</sup>, E. P. J. van den Heuvel<sup>1</sup>, Jorick S. Vink<sup>5</sup>, S. F. Portegies Zwart<sup>1,4</sup>, and A. de Koter<sup>1</sup>

<sup>1</sup> Astronomical Institute “Anton Pannekoek”, Kruislaan 403, NL-1098 SJ Amsterdam, the Netherlands

<sup>2</sup> Institute of Astronomy of the Russian Academy of Sciences, 48 Pyatnitskaya Str., 119017 Moscow, Russia

<sup>3</sup> Isaac Newton Institute, Moscow branch, 13 Universitetskii pr., Moscow, Russia

<sup>4</sup> Section Computational Science, Kruislaan 403, NL-1098 SJ Amsterdam, the Netherlands

<sup>5</sup> Armagh Observatory, College Hill, BT61 9DG, Northern Ireland, UK

received October 22, 2018

## ABSTRACT

**Context.** We study the evolution and fate of solar composition super-massive stars in the mass range 60 — 1000  $M_{\odot}$ . Our study is relevant for very massive objects observed in young stellar complexes as well as for super-massive stars that could potentially form through runaway stellar collisions.

**Aims.** We predict the outcomes of stellar evolution by employing a mass-loss prescription that is consistent with the observed Hertzsprung-Russell Diagram location of the most massive stars.

**Methods.** We compute a series of stellar models with an appropriately modified version of the Eggleton evolutionary code.

**Results.** We find that super-massive stars with initial masses up to 1000  $M_{\odot}$  end their lives as objects less massive than  $\simeq 150 M_{\odot}$ . These objects are expected to collapse into black holes (with  $M \lesssim 70 M_{\odot}$ ) or explode as pair-instability supernovae.

**Conclusions.** We argue that if ultraluminous X-ray sources (ULXs) contain intermediate-mass black holes, these are unlikely to be the result of runaway stellar collisions in the cores of young clusters.

**Key words.** Stars: evolution – supergiants – Stars: mass loss – Galaxies: star clusters

## 1. Introduction

In this paper, we study the structure and evolution of very massive stars (VMS), defined as objects with masses of 60 up to  $150 M_{\odot}$ , as well as super-massive stars (SMS) with masses in the range 150 - 1000  $M_{\odot}$ .

The interest in the upper limit of stellar masses and the evolution and fate of the most massive stars in the Universe was greatly boosted by the discovery of ultraluminous X-ray sources (ULX, see Fabbiano 1989; Colbert & Miller 2005; Fabbiano & White 2006; Fabbiano 2006; Soria 2006, and references therein). These objects are most commonly interpreted as binaries involving either sub-Eddington accretion onto an *intermediate mass black hole* (IMBH) with mass  $\sim (10^2 - 10^5) M_{\odot}$  or super-Eddington accretion onto a *stellar mass black hole* with mass  $\sim 10 M_{\odot}$ . In the latter case, beaming or support of super-Eddington luminosity by an accretion disk is required. Currently, the issue of the black hole masses in ULXs remains unresolved (see, e.g., Fabbiano 2006).

It has been argued that IMBHs may also reside in the cores of some globular clusters (see, e.g., Gerssen et al. 2002, 2003; Gebhardt et al. 2005; Patruno et al. 2006;

Feng & Kaaret 2006), but see Baumgardt et al. (2003a,b) for counter-arguments. The masses of the putative black holes in the cores of well-known globular clusters such as 47 Tuc and NGC 6397, are expected to be  $\sim (10^2 - 10^3) M_{\odot}$  (De Rijcke et al. 2006).

ULXs are observed in both spiral and elliptical galaxies, i.e. in environments with diverse metal abundances and star formation rates. In this paper, we focus on stars with solar initial composition ( $X=0.7, Z=0.02$ ). This choice is partly motivated by the high metallicity of the starburst galaxy M82 – with  $Z \simeq Z_{\odot}$  (McLeod et al. 1993; Origlia et al. 2004; Mayya et al. 2006) – which contains one of the most promising candidate ULXs, M82 X-1, and that may host a black hole of intermediate mass, as argued by e.g. Ptak & Griffiths (1999); Kaaret et al. (2001); Matsumoto et al. (2001); Strohmayer & Mushotzky (2003), but see Okajima et al. (2006) for arguments in favour of a stellar mass black hole in M82 X-1.

The current observational estimate of the upper cut-off of stellar masses is  $\sim 150 M_{\odot}$  (Massey & Hunter 1998; Weidner & Kroupa 2004; Figer 2005). However, for solar chemical composition, it is expected that even such massive stars rarely produce black holes more massive than

$\simeq 20 M_{\odot}$  (Maeder 1992; Fryer & Kalogera 2001), due to copious mass loss during both the hydrogen and helium burning stages. If ULXs and young globular clusters really harbour black holes with masses exceeding several  $10 M_{\odot}$ , the problem of their formation becomes a challenge for the theory of stellar evolution with mass loss.

Related intriguing problems involve the formation and evolution of the luminous stars found in the central parsec of the Galaxy, e.g., the S-stars and the IRS13 and IRS16 conglomerates (Schödel et al. 2005; Lu et al. 2004; Maillard et al. 2004)<sup>1</sup>, or in the R136 stellar complex of the 30 Doradus nebula in the Large Magellanic Cloud (Walborn & Blades 1997; Massey & Hunter 1998).

Returning to the problem of IMBH formation, there are currently two models in favour. One involves the gradual accumulation of mass by accretion onto a seed black hole, which, while swallowing gas and stars in a stellar cluster, may grow to the intermediate mass range (see, e.g., Miller & Colbert 2004, and references therein). The other scenario considers the collapse of an object which descends from an SMS formed by hierarchical runaway merger of ordinary stars in a young dense stellar cluster, during or after core collapse (see, e.g., Portegies Zwart et al. 1999; Portegies Zwart & McMillan 2002; McMillan et al. 2004; Gürkan et al. 2004; Portegies Zwart et al. 2004; Freitag et al. 2006).

The motivation for the current study stems from the latter scenario. It assumes that stars are born with a wide distribution of masses ranging from the hydrogen-burning limit up to a maximum of about  $150 M_{\odot}$ . More massive stars observed in the Galaxy may originate from stellar mergers. Most of these may be the result of coalescence of components of binaries in common envelopes. The mass of binary merger products may be up to  $300 M_{\odot}$ . Portegies Zwart et al. (1999); Miller & Hamilton (2002); Portegies Zwart et al. (2004); Gürkan et al. (2004) have demonstrated by means of detailed N-body simulations, in which simple stellar evolution was taken into account, that there is a range of initial conditions where stellar coagulation drives the mass of a star to  $\sim 1000 M_{\odot}$ . The resulting star burns up quite quickly, and the process of hierarchical merging in the cluster core terminates as soon as the first massive stars experience supernovae and collapse into black holes. The collision runaway process terminates as the mass loss from the explosions of massive stars in the cluster center drives the expansion of the cluster core. This scenario was used to explain the large black hole mass of M82 X-1 (Portegies Zwart et al. 2004).

The studies of hierarchical mergers take into account the possibilities of collisional mass loss, mass loss from stellar winds, and rejuvenation of merger products due to

fresh hydrogen supply in collisions. However, stellar evolution is treated rather crudely in these simulations, using extrapolations by several orders of magnitude for stars that typically have zero-age main-sequence (ZAMS) mass  $\leq 100 M_{\odot}$ . The possible formation of core-halo configurations and the existence of an upper stellar mass limit are generally ignored. The treatment of mass loss in stellar winds is particularly uncertain. In principle, the winds of very massive and super-massive stars may be so strong that the cluster core expands in such a dramatic way that it stops being dominated by collisions, in which case the hierarchical merger is terminated (Portegies Zwart et al. 1999; Vanbeveren 2005).

We aim to refine evolutionary calculations for merger products, and as a first step, we study the evolution of solar composition VMS and SMS over the mass range  $60$ – $1000 M_{\odot}$ . We construct chemically homogeneous models for these stars and confirm the existence of their upper mass limit ( $\simeq 1000 M_{\odot}$ ), and study their evolution with mass loss through the core hydrogen and core helium-burning stages. This allows us to determine the mass and nature of the pre-supernova objects and to predict the fate of these objects.

The results of our evolutionary computations are presented and discussed in Sect. 2, a comparison with observations is given in Sect. 3, the fate of SMS is discussed in Sect. 4. Conclusions of our study follow in Sect. 5. In the Appendix, we discuss a number of individual stars in close proximity to the Humphreys-Davidson (HD) limit.

## 2. The stellar evolution calculations

We compute the inner structure and evolution of single non-rotating SMS. Initially, all stars are chemically homogeneous. The products of hierarchical merging are expected to grow in mass in discrete steps by the injection of other stars and as a result the merger product may be rapidly rotating. In this paper, we ignore the effects associated with merger events themselves, but concentrate on the 1D (non-rotating) evolution of the final object, the super-massive star (SMS).

Another open question, which has persisted for decades, is that of the pulsational stability of SMS (see, e.g., Baraffe et al. 2001). Existing nonlinear calculations of the effects of pulsations on mass loss differ by an order of magnitude. Appenzeller (1970) found that pulsationally-driven mass loss for solar metallicity stars with  $M \geq 300 M_{\odot}$  occurs on a timescale that is shorter than the core-hydrogen burning timescale, but Papaloizou (1973) claimed that the mass-loss rate is an order of magnitude lower and evolutionarily insignificant. Wolf-Rayet (WR) stars and luminous blue variables (LBVs) are the descendants of main-sequence stars and are likely to be subject to pulsational instabilities (Fadeyev & Novikova 2004). Awaiting the resolution of this problem, we do not explicitly consider the possibility of vibrational mass loss in our calculations.

<sup>1</sup> Note that a high stellar mass inferred from luminosity may be an artifact of unresolved binarity. For instance, IRS16 SW turned out to be a binary with two almost identical components of  $\sim 50 M_{\odot}$ , (DePoy et al. 2004; Martins et al. 2006; Peebles et al. 2007).

The evolutionary computations were carried out by means of an appropriately modified version of the Eggleton (1971, priv. comm. 2003) evolutionary code. The input physics has been described in Pols et al. (1995), but here we briefly list the sources of opacities and nuclear rates. The opacity tables are constructed using OPAL tables of Iglesias & Rogers (1996), low-temperatures opacities are from Alexander & Ferguson (1994), whilst Hubbard & Lampe (1969) and Itoh et al. (1983) list conductivities for degenerate matter. The nuclear evolution of  $^1\text{H}$ ,  $^4\text{He}$ ,  $^{12}\text{C}$ ,  $^{14}\text{Ne}$ ,  $^{16}\text{O}$ ,  $^{20}\text{Ne}$ ,  $^{24}\text{Mg}$  is followed using the reaction rates from Caughlan & Fowler (1988) and Caughlan et al. (1985). The equation of state is based on the principle of Helmholtz free energy minimisation and provides the physical quantities such as the pressure, density, specific heats etc. as a function of a parameter related to the electron degeneracy and temperature.<sup>2</sup>

An initial solar chemical composition ( $X=0.7$  and  $Z=0.02$ ) is assumed, and the computations may be relevant to the Galactic objects such as the most massive members of Arches, Quintuplet, IRS13, IRS16, NGC3603, Westerlund clusters (see, e.g., Portegies Zwart 2004, for further references) and, in case they do exist, to SMS in those external galaxies that have chemical abundances comparable to the composition of the Milky Way. We consider stars with surface helium abundance  $Y_c \geq 0.4$  and  $T_{\text{eff}} \geq 10000\text{ K}$  to be WR stars.

### 2.1. Homogeneous supermassive stars

With the opacity increasing outwards, a star develops a structure where most of the mass is concentrated in the compact convective core, whilst only a small fraction of the mass is located in a very extended radiative envelope (“core-halo configuration”, Kato 1985, 1986). More massive stars tend to be more extended, and the expansion of the envelope is caused by the increase of the Eddington luminosity  $L_{\text{Edd}} = 4\pi cGM_r/\kappa$ , where  $\kappa$  is the flux-mean opacity in the radiative outer layers of the star. The maximum mass for a stable star is reached when the luminosity of the star reaches  $L_{\text{Edd}}$  in the photosphere. Using Compton scattering opacity  $\kappa = 0.2(1+X)/(1+2 \times 10^{-9}T)$ , Kato succeeded in constructing homogeneous hydrogen-rich solar metallicity stellar models of  $10^7 M_\odot$ . The inclusion of the Kramers term in the opacity resulted in a reduction of the limiting ZAMS mass to  $\approx 10^6 M_\odot$  (Menshchikov & Tutukov 1989). These last authors also found an upper limit of about  $2500 M_\odot$  for helium-rich stars ( $X=0$ ,  $Y=0.97$ ).

Ishii et al. (1999) explored the core-halo effect using modern OPAL opacities and found that, in this case, the upper mass limit for hydrogen-rich stars drops drastically. For stars of solar composition, this limit is reached at a

mass of about  $1000 M_\odot$ , and at a somewhat lower mass for stars with lower metallicity.

If  $\Gamma \equiv L/L_{\text{Edd}} \rightarrow 1$  in the interior of a 1-D stellar model, the radiative pressure can be balanced by a density inversion (see, e.g., Langer 1997). In our calculations, the highest luminosity is reached for homogeneous models for  $M \approx 1001 M_\odot$ . In this case,  $\Gamma \approx 0.98$  in the outermost meshpoint in the stellar model (see Fig. 1). A further increase of the stellar mass is then not possible, since the convection in the surface layers is insufficient to transport the stellar luminosity, and density inversions cannot build up.

If stars rotate and the critical velocity of rotation behaves as  $v_{\text{crit}} \propto (1 - \Gamma)^{0.5}$ , critical rotation is achieved before  $\Gamma$  reaches unity for any rotational velocity (Langer 1997). For rotating stars, the actual upper mass limit for solar metallicity may therefore be lower than  $1000 M_\odot$ .

The development of a core-halo structure leads to a bending of the sequence of homogeneous stars towards the red in the HRD. In our models, this bending occurs above a mass  $\simeq 133 M_\odot$  in agreement with e.g., Figer et al. (1998); Ishii et al. (1999); Stothers & Chin (1999).

An approximate mass-luminosity relation for  $(100 - 1000) M_\odot$  homogeneous stars obtained in the present study is (in solar units):

$$L \simeq 10^{3.48} M^{1.34}. \quad (1)$$

For the  $(25 - 115) M_\odot$  initial mass range, the mass-radius relation may be approximated as

$$R \simeq 10^{-0.9} M^{1.02}, \quad (2)$$

and for larger masses as

$$R \simeq 10^{-0.77} M^{0.96} \quad (3)$$

We note that although we can theoretically construct this sequence of completely homogeneous massive star models, in reality, stars may form by accretion, and stars could start core hydrogen burning before accretion halts, and evolve along the main-sequence until the accretion reservoir becomes exhausted (see, e.g., Behrend & Maeder 2001).

### 2.2. The mass-loss rate

Massive stars are subject to considerable mass loss, driven mainly by radiation pressure through spectral lines, which can be enhanced by currently poorly understood vibrational modes. For stars more massive than  $\sim 100 M_\odot$  theoretical models are not yet well developed. Kudritzki (2002) calculated mass-loss rates for masses up to  $300 M_\odot$ , but the mass-loss rates of Kudritzki do not include the important effect of multi-line scattering, which may be vital for models in close proximity to the Eddington limit. Vink (2006) presented mass-loss predictions for very massive stars close to the Eddington limit, and found a steep behaviour of the mass-loss rate as a function of  $\Gamma$  (but for

<sup>2</sup> The most recent updates may be found at <http://www.ast.cam.ac.uk/~stars/>

a constant ratio of the terminal velocity over the escape velocity).

We did not use the mass-loss rates of Vink et al. (2000) for stars above  $100 M_{\odot}$ , as they were derived for  $\Gamma < 0.5$ . As the Vink et al. recipe includes bi-stability jumps, which are a function of  $T_{\text{eff}}$  and wind density (and hence  $\Gamma$ ), we did not extrapolate the Vink et al. recipe outside its validity range.

A break of evolutionary sequences occurred in calculations for massive stars by other authors with mass-loss prescriptions based on radiation-driven wind models (e.g., for Pistol star by Figer et al. 1998). The extrapolation of fits to the empirical data on mass-loss rates (de Jager et al. 1988) for stars more massive than  $\simeq 120 M_{\odot}$  results in unreasonably high mass-loss rates, causing the stellar evolution models to lose their ability to converge.

Due to the sparsity of theoretical expressions for the amount of mass loss from supermassive stars, we adopt the following *ad-hoc* “momentum” equation for our evolutionary models:

$$\dot{M} = \frac{L}{v_{\infty} c} \frac{1}{(1 - \Gamma)^{(\alpha - 0.5)}}, \quad (4)$$

where  $L$  is the stellar luminosity,  $v_{\infty}$  is terminal velocity of stellar wind,  $c$  is the speed of light, and  $\Gamma = L/L_{\text{Edd}}$  in the outermost meshpoint of the stellar model. After Kudritzki & Puls (2000) we define

$$v_{\infty} = C(T_{\text{eff}}) [(2GM/R)(1 - \Gamma)]^{0.5}. \quad (5)$$

We do not specify a particular physical mechanism for our mass-loss prescriptions, but the luminosity dependence in Eq. (4) accounts for the assumption that radiation pressure almost certainly plays a role. Furthermore, we account for the proximity to the Eddington limit by introducing the  $L/L_{\text{Edd}}$  dependence. We have tested our Eq. (4) against the Vink et al. (2000) mass-loss recipe for a  $60 M_{\odot}$  star, and although there are differences due to the presence of bi-stability jumps in the Vink et al. recipe, which we do not account for in our mass-loss prescription, the overall mass lost ( $35 M_{\odot}$ ) is very similar, bringing a  $60 M_{\odot}$  star down to  $25 M_{\odot}$ .

As noted by Vink et al. (2001), while the metal lines are responsible for driving the wind, hydrogen and helium lines are sparsely populated in the spectral range where early-type stars emit most of their energy. This provides some justification for using the same mass-loss recipe for hydrogen-rich stars, as well as for stars with hydrogen-exhausted atmospheres.

We base our choice of  $\alpha$  in Eq. (4) on two criteria: 1) stars should spend most of their lifetime between the ZAMS and the HD-limit (as defined in Humphreys & Davidson 1994), and 2) they should spend only a limited amount of time, e.g. less than  $\sim 1 - 2\%$  of their lifetime, at effective temperatures cooler than the Humphreys-Davidson limit. The nature of the Humphreys-Davidson limit is still elusive, as it is still unclear whether the lack

of stars above this empirical limit is due to physical processes (likely to be related to the Eddington limit), or it has a statistical nature instead. As some stars are observed on the cool side of the HD-limit (see Fig. 11), we consider the possibility that the evolutionary tracks extend to the yellow and red regions of HR-diagram.

We present our simulations for 60 and  $120 M_{\odot}$  stars in Fig. 2 and Table 5.

For  $\alpha = 0.25$ , the  $M_0 = 60 M_{\odot}$  star loses  $23.5 M_{\odot}$  during the core-hydrogen burning phase that lasts for 3.8 Myr. At the TAMS, the surface hydrogen and helium abundances are virtually equal  $X \approx 0.49$  and  $Y \approx 0.49$ , and  $C/N$  and  $O/N$  ratios are very close to their nuclear equilibrium values (see Fig. 13 below). The star may be classified as a strongly helium-enriched O-star. A further  $12 M_{\odot}$  are lost in the part of the track where the stellar effective temperature is below  $\simeq 10\,000\text{K}$ , with a lifetime in this later stage of 0.048 Myr. When the star crosses the HD-limit moving blueward, the hydrogen abundance at its surface is 0.096, and the object has become a WR star.

This track agrees well with the track for which we used the mass-loss prescription of Vink et al. (2000), where the mass-loss behaviour is not completely continuous due to the presence of bi-stability jumps. The total amount of mass lost during the main-sequence phase is  $19.4 M_{\odot}$ , whilst  $13 M_{\odot}$  is lost when star is cooler than  $\sim 10\,000\text{K}$ . The lifetime of the later stage is 0.088 Myr. This compares well to the results of Limongi & Chieffi (2007), who used the mass-loss rates from Vink et al. (2000) and found a total amount of mass loss of  $\Delta M = 22 M_{\odot}$  during the main-sequence stage.

The  $M_0 = 120 M_{\odot}$  star, computed with  $\alpha = 0.25$ , loses  $\simeq 57 M_{\odot}$  over its 2.76 Myr long main-sequence lifetime. While on the cool side of the HD-limit (at  $T_{\text{eff}} \lesssim 30\,000\text{K}$ ), the star loses an additional  $\simeq 14 M_{\odot}$  in 0.039 Myr. In the latter case, the star becomes a WR object during the main-sequence (see more below).

The last models of the sequences for stars with initial masses 60 and  $120 M_{\odot}$  are in the core He exhaustion phase (Table 5), with masses of  $\simeq 40 M_{\odot}$  and  $\simeq 21 M_{\odot}$ , respectively. These values are in reasonable agreement with the masses of  $\simeq 30 M_{\odot}$  and  $\simeq 20 M_{\odot}$ , obtained by Limongi & Chieffi (2007) who used mass-loss rates from Vink et al. (2000) for blue supergiants, from de Jager et al. (1988) for red supergiants, and from Nugis & Lamers (2000) for WR stars. We also note that the tracks computed by Limongi & Chieffi (2007) for 60 and  $120 M_{\odot}$  stars penetrate into the cool region of the HR-diagram to  $\log T_{\text{eff}} \approx 3.65$  and 3.70, respectively, again in good agreement with our computations.

Finally, our tracks for  $\alpha = 0.25$  are in reasonable agreement with the tracks computed using the spline fits of de Jager et al. (1988) for empirical  $\dot{M}$  but, as we mentioned above, the latter fits diverge at high stellar masses.

For  $\alpha = 0.1$ , the  $M_0 = 120 M_{\odot}$  star crosses the Humphreys-Davidson limit during core-hydrogen burn-

ing, and spends  $\sim 0.5$  Myr in the low-temperature region, which is too long.

Based on this analysis, we conclude that  $\alpha \simeq 0.25$  is suitable for evolving supermassive stars and we adopt this value throughout the paper.

### 2.3. Evolution of supermassive stars

A summary of the parameters of evolutionary tracks computed in the present paper is given in Table 5. Figure 3 shows evolutionary tracks for stars with initial masses 60, 120, 200, 500, and  $1001 M_\odot$ , computed for different values of the parameter  $\alpha$ .

For  $\alpha \geq 0.5$ , the mass-loss timescale is shorter than the nuclear evolution timescale. The stars evolve downward along the locus of homogeneous stars remaining practically unevolved (Figs. 3,4). For all sequences, the mass-loss rate is so high that nuclear-processed layers are almost immediately exposed at the surface. For stars with  $M_0=500$  and  $1001 M_\odot$ , when central hydrogen becomes exhausted, the surface abundance of hydrogen is just several per cent. Thus, SMS turn into WR stars during the core hydrogen burning stage.

For models with high  $\alpha$ , the bending of the evolutionary tracks to higher  $T_{\text{eff}}$  (bottom loop) starts when  $X_c \simeq 0.05$  in the convective core, i.e. this corresponds to what, in the common notation, would be “point B” of the evolutionary track. The blue points of the loops of the tracks for  $\alpha \geq 0.5$  correspond to the core hydrogen exhaustion. The direction of evolutionary tracks changes from redward to blueward, when the core He-burning becomes the dominant source of energy:  $L_{\text{He}}/L_H \sim 3$ . For all models, the stars evolve into virtually identical helium stars, as the stellar evolution converges. The evolutionary tracks start to deflect from the ZAMS to the right only for  $\alpha \leq 0.5$ . These high- $\alpha$  tracks may be relevant for the evolution of putative SMS ( $M \gtrsim 120 M_\odot$ ), but they are less relevant for known VMS ( $M \lesssim 120 M_\odot$ ).

The behaviour of the evolutionary sequences with high mass-loss rates is consistent with the results of Maeder (1980), who showed that stars with an initial mass in excess of  $100 M_\odot$ , and with a time averaged  $\dot{M} \gtrsim 2 \times 10^{-5} M_\odot \text{ yr}^{-1}$  evolve towards the left of the HR diagram. In the interior, a large homogeneous core is surrounded by an envelope with very little difference in composition between the core and the stellar surface. Stothers & Chin (1999) used OPAL opacities and found a similar convergence of the evolutionary tracks.

To be consistent with restrictions upon the mass-loss rates found by evolutionary computations for  $M_0 = 60$  and  $120 M_\odot$  stars (§ 2.2), we now discuss the tracks for  $\alpha = 0.25$ . The behaviour of all evolutionary sequences is rather similar. For high  $\alpha$  ( $\alpha=1$ ; Fig. 4) the tracks converge quicker than for our favourite  $\alpha=0.25$  models (Fig. 5). Figure 5 represents the relations between evolutionary time, the mass of the star, the central hydrogen abundance and the surface helium abundance for

$\alpha = 0.25$ . For the  $M_0=200$  and  $120 M_\odot$  models, the hydrogen surface abundances for  $X_c = 0$  are 0.12 and 0.25, respectively. If we consider the surface helium abundance,  $Y \approx 0.4$ , as a conventional threshold for assigning the WR spectral type, this limit is reached within  $\lesssim 1$  Myr for stars with  $M \geq 200 M_\odot$ , whilst it takes about 2 Myr for the  $120 M_\odot$  star.

Figures 6 and 7 show that after the end of the central H-burning all stars start to expand on the thermal time scale of their envelopes. Expansion is accompanied by a strong reduction of  $L/L_{\text{Edd}}$ : although the stellar  $L$  remains practically the same, the  $L_{\text{Edd}}$  of the outermost meshpoint increases rapidly due to a reduction in opacity. The reduction of  $\Gamma = L/L_{\text{Edd}}$  would increase the mass-loss rate if it were to act alone. However, our adopted mass-loss prescription depends weakly on  $\Gamma$ . The decisive factor in Eq. (4) is  $v_\infty$ , which decreases strongly with the expansion of the star, causing the growth of  $\dot{M}$ . A further mass and gravity reduction at almost constant luminosity results in a kind of runaway mass loss, i.e., the star becomes unstable. The expansion terminates when the core He-burning becomes the dominant source of stellar luminosity. The star then returns rapidly to the blue region of the HR-diagram. In our calculations mass loss occurs continuously. In real stars, one may expect that instability associated with high  $L_{\text{Edd}}$  would manifest itself as a sequence of sporadic mass-loss episodes which terminate when He-burning causes an overall contraction of the star. We may speculate that the total amount of mass lost in the “spike” of the mass-loss rate during redward excursions is similar to that which would be lost by a “real” star in a series of outbursts. The total stellar luminosity becomes very close to the Eddington luminosity when the star returns to the high  $T_{\text{eff}}$  region of the HR-diagram.

An interesting feature of SMS evolution is the increase of the core hydrogen-burning time of the stars with increasing  $\alpha$  in the mass-loss prescription. This is understandable, as heavy mass loss is accompanied by a reduction of the central temperature and density (like in close binary components that experience dynamical- or thermal-timescale mass loss upon Roche lobe overflow).

Figure 8 shows that irrespective of initial stellar mass, for  $\alpha = 0.25$ , the maximum mass-loss rates do not exceed the maximum mass-loss rate for line-driven winds. Smith & Owocki (2006) recently estimated this maximum to be:

$$\dot{M} \approx 1.4 \times 10^{-4} (L/(10^6 L_\odot)) M_\odot \text{ yr}^{-1}. \quad (6)$$

A similar order of magnitude ( $10^{-3} M_\odot \text{ yr}^{-1}$ ) estimate for the upper limit of  $\dot{M}$  due to radiation pressure on spectral lines was obtained by Aerts et al. (2004). Figure 9 shows the run of the “wind performance number”  $\eta = (\dot{M} v_\infty)/(L/c)$ , along evolutionary tracks for model sequences with  $\alpha = 0.25$ .

One of the main results in the section is the finding of the convergence of our models with a wide range of initial masses (see Fig. 5). This convergence of stellar masses

which initially differ by a factor  $\sim 10$  may crudely be explained as follows. During most of the stellar lifetime the value of  $L/L_{\text{Edd}}$  is not far from 1 (see Fig. 7), whilst the stellar radius changes significantly for only a very short time. Therefore, the crucial factor that sets the rate of mass loss is the stellar luminosity, which may, as a first approximation, be taken as the luminosity of a homogeneous star. For the case of  $\alpha = 0.25$ , the stellar lifetime is  $t \approx 10^{6.9} (M/M_{\odot})^{-0.2} \text{ yr}$  (for  $120 M_{\odot} \leq M_0 \leq 1000 M_{\odot}$ ). When we now apply the mass-luminosity relation, the amount of mass lost,  $\Delta M$ , is found to be comparable to the initial mass of the star,  $M_0$ .

### 3. Models of VMS versus observed stars

Figure 6 shows the mass-loss dependence on time for  $\alpha = 0.25$  sequences and compares them with the mass-loss ranges found for young massive stars in the Arches and Quintuplet clusters, and the cluster of HeI-emission stars in the Galactic center, as well as for a sample of WNLh stars in young massive clusters in the Milky Way and the Magellanic Clouds (A. de Koter, unpublished). In Figure 10, we show in detail the relations between stellar mass and the mass-loss rate for  $\alpha = 0.25$  evolutionary sequences for objects with initial masses of 60, 120, and  $200 M_{\odot}$ , and we compare them with mass-loss prescriptions suggested for massive stars, as well as with observations of known objects. We remind the reader that we consider stars with surface helium abundance  $Y_c \geq 0.4$  and  $T_{\text{eff}} \geq 10000 \text{ K}$  to be WR stars.

A fit for observed mass-loss rates of O-stars is given by de Jager et al. (1988). For  $M > 120 M_{\odot}$ , comparing models with any observational data fits is not very sensible, because it would involve too rough an extrapolation. However, our mass-loss rates for the  $M_0 = 120 M_{\odot}$  star, when it is still H-rich, do not contradict the fits of de Jager et al. (1988), nor the observations of the most massive H-rich WR-stars.

For WR-stars, fits to observational data were given by e.g. Langer (1989)<sup>3</sup>:

$$\dot{M} = -2 \times 10^{-8} M^{2.5};$$

Nelemans & van den Heuvel (2001):

$$\dot{M} = -1.4 \times 10^{-8} M^{2.87};$$

de Donder & Vanbeveren (2003)<sup>4</sup>:

$$\log(-\dot{M}) = \log L - 10$$

<sup>3</sup> The numerical coefficient in Langer's formula is taken to be three times lower than the originally suggested lowest coefficient, to account for wind clumping (Hamann & Koesterke 1998; Marchenko et al. 2007).

<sup>4</sup> For the most massive WR stars, this fit gives rates close to the ones suggested by the Nugis & Lamers (2000) fits. In Fig. 10, the original formula is extrapolated to higher stellar masses.

(solar units and rates per yr are used). In Fig. 10, we also show observational estimates for mass-loss rates of WN stars with  $M \geq 20 M_{\odot}$  from Hamann et al. (2006). Estimates of  $\dot{M}$  for WR stars (Hamann et al. 2006) shown in Fig. 10 agree well with the estimates of Cappa et al. (2004), based on radio-observations that showed that  $\dot{M}_{\text{WR}}$  hardly exceeds  $10^{-4} M_{\odot} \text{ yr}^{-1}$ . Figure 10 clearly shows that extrapolation of the formulae given above to very massive WR stars is not justified. Late-type WN stars like WR20a (see Appendix for more details) may still be in their core-hydrogen burning stage.

In Figs. 11 and 12, we present evolutionary tracks for  $\alpha=0.25$  and  $0.5$  sequences in the HR-diagram and we compare them to the positions of some of the most luminous stars in the Milky Way and the Magellanic Clouds (Table 2). For notes on the individual stars shown in Figs. 11 and 12, we refer the reader to the Appendix. These figures indicate quite clearly that  $\alpha = 0.5$  would be too high a value, and that  $\alpha$  should be  $\sim 0.25$  to be consistent with the observations.

The data presented in Figs. 6, 10, 11, and 12 suggest that the initial masses of the stars observed in the Arches cluster, Quintuplet and R136 may exceed  $\simeq 100 M_{\odot}$ . Shortly after leaving the ZAMS, these stars acquire surface abundances that result in their spectral classification as transitional types between O-stars and WR stars. The positions of luminous stars with estimated  $M$  and  $\dot{M}$  in Figs. 10 and 11 suggest that they have initial masses up to  $\sim 100 M_{\odot}$ , and are in the core-hydrogen burning stage. The positions of these objects in the  $(M - \dot{M})$ -plots and the HR-diagram are consistent. This point may be further explored when more detailed grids of evolutionary tracks become available. We note that masses and the estimates for  $\dot{M}$  are both uncertain. For instance, Repolust et al. (2004) estimate the range of uncertainty of their spectroscopic mass determinations for Galactic O-stars (listed in Table 2) as  $^{+50}_{-30}\%$ . For the mass-loss rates, the errors are up to 0.2dex.

The mass-loss rates that we obtained for pure helium stars have the same range as  $\dot{M}$  for hydrogen-rich stars. This is consistent with the similarity of  $\dot{M}$  values found for O-stars and HeI-emission stars, of which some are helium rich<sup>5</sup>, but it does not seem to agree with the Hamann et al. (2006) data for hydrogen-poor WR stars.

We should note that we obtain higher masses for WR stars and pre-supernovae masses than in some previous computations for non-rotating stars. For instance, for the same  $120 M_{\odot}$  star, Schaller et al. (1992) obtain  $\simeq 7.6 M_{\odot}$  at the end of their calculations, whilst our computations yield a final mass of  $40.4 M_{\odot}$  (for  $\alpha = 0.25$ ). The difference stems from the difference in mass-loss rates for He-rich stars. For the latter, Schaller et al. use the rates from Langer (1989), uncorrected for clumping, that are much higher than those given by our empirical algorithm for  $\dot{M}$ .

<sup>5</sup> The estimates of  $\dot{M}$  for HeI stars strongly depend on an uncertain He/H-ratio.

In Fig. 13, we show the evolution of the chemical abundances at the surface of a  $60 M_{\odot}$  VMS and a  $500 M_{\odot}$  SMS. We note several differences in the behaviour of the surface abundances. On the surface of the  $M_0 = 60 M_{\odot}$  star, helium starts to dominate over hydrogen only close to the TAMS, whilst for the  $M_0 = 500 M_{\odot}$  SMS, this already happens much earlier. This difference is due to the relative sizes of the convective cores. Furthermore, the surface of the VMS becomes enriched in nitrogen (relative to the solar abundance) close to the TAMS, and remains so until the end of the helium exhaustion of the core. For this case, we expect the pre-supernova object to be a WN star.

The surface layers of the SMS become enriched in nitrogen almost immediately after the departure from the ZAMS. Later, at the TAMS<sup>6</sup>, the hydrogen and nitrogen abundances drop almost simultaneously, and the surface becomes dominated by He and C. In the final stages of evolution, oxygen becomes the dominant surface element, whilst the abundance of helium becomes even lower than that of carbon. In this case, the expected pre-supernova object is an oxygen-carbon star, with traces of helium at the surface.

Figure 13 also shows the differences in the surface CNO-cycle element ratios of VMS and SMS. For the latter, the layers in which the elements are in nuclear equilibrium are exposed virtually immediately at the beginning of their evolution (after the loss of only about  $100 M_{\odot}$  in only  $\simeq 0.7$  Myr). This situation persists until C and O enriched layers become exposed due to He-burning. As the core H-burning evolutionary stage is by far the longest, we conclude that a majority of SMS should have nuclear-equilibrium ratios of CNO-elements.

For the case of the VMS, the transition in chemical abundance from solar to nuclear-equilibrium occurs somewhat more smoothly. It starts after about 2 Myr of evolution, whilst it takes about 2 Myrs out of a total 6 Myrs MS-lifetime. During this transitional phase, the star loses about  $10 M_{\odot}$ . If our mass-loss algorithm is applicable to the lower mass VMS, we should expect this transition to occur smoothly. VMS close to the TAMS are expected to be associated with luminous blue variables (LBVs), for which a wide span of CNO-elements ratios has been found. Although Smith et al. (1998) found LBV ejecta to be N-enriched, these have generally not yet reached CNO equilibrium values. However, as there is controversy about the origin of LBV nebulae, it would arguably be better, or at least more direct, to consider photospheric abundances instead. These, however, may depend on complexities of the atomic physics and wind analyses, and the results are conflicting. For instance, evidence for advanced nuclear processing was found by Lennon et al. (1993) for the LBV R71 in the LMC, but this is not a well-established fact for LBVs as a population. Although most LBVs show CNO-

enriched atmospheres, it seems unlikely that all of them have already reached their CNO equilibrium values.

A range of CNO abundances may naturally be explained from our VMS computations, but given that most LBV masses are not significantly over  $150 M_{\odot}$ , it seems unlikely that all LBVs are the progeny of SMS, as our models would predict SMS to reach CNO equilibrium almost instantaneously.

#### 4. The fate of supermassive stars

According to our evolutionary calculations, SMS transform into oxygen-neon stars with traces of carbon. Depending on the progenitor mass, the final masses of the stars are between  $\simeq 20 M_{\odot}$  and  $\simeq 140 M_{\odot}$ . One may expect that further reduction of the total stellar mass would be negligible, because of the short lifetime of stars in their post core-helium burning evolutionary stages. The helium-carbon-oxygen outer layer comprises only a few per cent of the total mass of the star. Thus, one may expect that if these objects were to explode, SMS would probably produce type Ic events.

It has been known for decades (see, e.g., pioneering papers of Rakavy & Shaviv 1967; Fraley 1968; Ober et al. 1983, and many other studies) that if the mass of oxygen stars exceeds several tens of  $M_{\odot}$ , during central oxygen-burning, they enter the electron-positron pair instability regime, and contract quasi-dynamically. When the central temperature increases to  $(3 - 6) \times 10^9$  K, central oxygen burning becomes explosive, which is much faster than neutrino energy losses. The released nuclear energy may be sufficient for the internal energy to exceed the gravitational binding energy. The star will then disrupt completely, without leaving a compact remnant, giving rise to a so-called “pair-instability (or pair-creation) supernova” (PISN). If the released energy is not large enough to disrupt the star, the star collapses to a black hole. This instability arises irrespective of the metallicity of the progenitor star. However, for solar composition stars the possibility of PISN is usually not considered, since in the evolutionary models for even the most massive stars formed in the “standard” way (i.e. without possible runaway collisions), with masses up to “observational” upper limit of  $150 M_{\odot}$ , sufficiently massive oxygen cores are not formed. We note that this may stem from an overestimate in the mass-loss rates during the WR-stage (if mass-loss prescriptions like those shown in Fig. 10 are extrapolated).

However, massive oxygen cores are more often considered in relation to the evolution of Population III stars. Massive oxygen cores may experience only moderate mass loss, owing to the absence of metals (but see Vink & de Koter 2005 and Vink 2006 for a discussion on the possibility of higher mass loss due to the radiative driving through intermediate mass CNO elements, and the likely proximity to the Omega/Eddington limit). One may use the results obtained for Pop. III stars for solar composition stars, because of a rather modest difference in internal structure of massive stars of different initial metallicity

<sup>6</sup> With the caveat that we use the definition of the TAMS in a broad sense indicating the end of the core hydrogen-burning stage.

during the late stages of evolution (e. g., Schaller et al. 1992). Umeda & Nomoto (2002) find, in computations for Pop. III stars, that PISNs are experienced by stars that form He-cores with mass  $(70 - 129) M_{\odot}$ . A similar range of  $(63 - 133) M_{\odot}$  was found by Heger & Woosley (2002) from computations of non-rotating He-stars. Apart from differences in the input physics, some discrepancy in mass obtained by different authors stems from the well-known fact that the evolution of initially naked helium stars is slightly different from the evolution of similar mass helium cores of stars formed through hydrogen burning. Stars that have helium cores more massive than the ranges of PISN-progenitors quoted above form black holes without ejecting matter. Stars with He-core masses below these limits are expected to collapse directly to a black hole or form a black hole through fall-back (Fryer 1999).

In Fig. 14, we plot the initial-final mass relation for SMS, using the results of Umeda & Nomoto (2002) and Heger & Woosley (2002), and we mark approximate boundaries between regions with different outcomes. These boundaries are rather crude, but they suggest the following: we hardly expect the formation of black holes with masses larger than  $\sim 150 M_{\odot}$ . As the difference between the upper mass boundary of PISN-producing SMS ( $\sim 800 M_{\odot}$ ) and the upper SMS initial mass limit ( $\sim 1000 M_{\odot}$ ) is quite small, black holes with masses larger than PISN-producing objects may hardly form, and it is quite likely that the most massive black holes produced by SMS have only  $M \lesssim 70 M_{\odot}$ .

Figure 15 shows the lifetimes of supermassive stars. It is worth noting that lifetimes of SMS may be shorter than the 3 Myr usually assigned to the most massive stars, and this may be relevant for studies of the upper limit of nascent stars that use age-related arguments (e.g. Figer 2005).

## 5. Summary and discussion

In this paper we discuss the evolution of stars with initial masses in the range  $60 M_{\odot}$  to  $1001 M_{\odot}$ . Our study was motivated by the results of the direct  $N$ -body simulations of dense star clusters by Portegies Zwart et al. (1999), in which a star grows by repeated collisions to well beyond  $100 M_{\odot}$ . In later studies, Portegies Zwart et al. (2004) proposed that the collision runaway in star clusters could explain the presence of a black hole of  $\gtrsim 600 M_{\odot}$  in the star ULX M82 X-1 in cluster MGG11, which supposedly could have formed from a  $\gtrsim 1000 M_{\odot}$  star. According to these models, the mass of the VMS increases over the stellar lifetime, starting as a homogeneous massive  $\sim 100 M_{\odot}$  star that grows to  $\gtrsim 1000 M_{\odot}$  within the core-hydrogen burning stage of evolution.

We have assumed that our stellar evolution calculations are representative for stars that grow in mass via the collision runaway process. This is not necessarily correct, as the hydrogen reservoir of the collision runaway product will continuously be replenished by repeated collisions, whereas in our simulations we start with a high-mass ho-

mogeneous model. Furthermore, rotation may play a relevant role in the evolution of these objects, which was also ignored in our study. Having noted this, we may nonetheless expect these massive objects to be subject to heavy mass loss, and we may provide meaningful results in terms of the fate of the objects under consideration.

We have confirmed previous results on the existence of an upper mass limit for chemically homogeneous stars, which is reached when the luminosity in the outermost layers of the stars approaches the Eddington luminosity, at which point gravity is unable to balance radiation pressure. For non-rotating solar composition stars, this limit is reached at about  $1000 M_{\odot}$ . We evolved the stars of  $60 M_{\odot}$  to  $1001 M_{\odot}$  to the end of the core helium-burning stage and calibrated the stellar mass-loss prescription adopted by enforcing the condition that no star should spend more than a few percent of its life above the HD-limit. We found that mass-loss rates and HR-diagram positions of the earliest O-type stars, and stars classified as transitional between O- and WR-stars, may be consistent with our computed tracks.

Based on our mass-loss prescription and stellar evolution calculations, we argue that the observed massive stars in the Galaxy and the Magellanic Clouds had birth masses of up to  $\simeq 200 M_{\odot}$ . For stars in the lower part of this mass-range, mass loss during the MS-stage leads to the exposure of layers moderately enriched in He, and they may be observed as late-type WN stars with hydrogen features in their spectra. In the upper part of this range, stars become hydrogen-deficient WR stars already on the main-sequence.

Recently, Belkus et al. (2007) published a study of the evolution of stars with masses up to  $1000 M_{\odot}$ . Our study differs from that of Belkus et al. in two important aspects: (i) they provided a simple evolutionary recipe based on similarity theory, assuming that stars are homogeneous throughout the entire course of their evolution due to vigorous convection and stay in thermal equilibrium, whereas we present detailed stellar structure models; (ii) Belkus et al. used extrapolated mass-loss rates as predicted from radiation-driven wind theory, whilst we employed a mass-loss prescription that is consistent with the location of the most massive stars in the Hertzsprung-Russell diagram. In both studies, it is found that SMS are subject to dramatic mass loss that probably inhibits the formation of IMBH by the runaway stellar collision scenario.

Star clusters that experience core collapse before the most massive stars have left the main-sequence can develop a supermassive star via collision runaway. The mass of such an object is accumulated in subsequent collisions on a time scale of less than 3 Myr. The mass which can be grown in this time interval can be estimated using Eq. (2)



of Portegies Zwart et al. (2006)<sup>7</sup>:

$$m_r \simeq 0.01m \left(1 + \frac{t_{r1}}{100 \text{ Myr}}\right)^{-1/2}, \quad (7)$$

where  $m_m$  is the mass of the object formed by run-away collision,  $m$  is the system mass, and  $t_{r1}$  is the system relaxation time. The average mass increase per collision is about  $\sim 20 M_\odot$  (Portegies Zwart et al. 1999) (for a more complete discussion, however, see Portegies Zwart & McMillan (2002)). The supermassive star that accumulates  $\sim 1000 M_\odot$  has experienced some 45 collisions between the moment of gravothermal collapse of the cluster and the moment that the supermassive star dies. The mean time between collisions for this model is  $\lesssim 6.0 \times 10^4$  years, resulting in a mass accretion rate of  $\gtrsim 3 \times 10^{-4} M_\odot/\text{yr}$ . This rate of mass accretion is lower than the rate of mass loss that we get for the most massive stars ( $\sim 3.8 \times 10^{-3} M_\odot/\text{yr}$ ), but since these numbers of mass-accretion and mass-loss rate are quite uncertain, it is not inconceivable that, in spite of the strong stellar winds, the objects may nonetheless experience a net gain in mass during their lifetimes. This conclusion was drawn by Suzuki et al. (2007) who recently studied stellar evolution with mass loss of collisionally merged massive stars. They concluded that stellar winds would not inhibit the formation of SMS. We note, however, that the Suzuki et al. (2007) calculations were limited to masses up to  $\sim 100 M_\odot$  and their calculations did not consider the more important effect of mass loss for the final mass growth process, where the mass is supposed to increase beyond this value of  $100 M_\odot$  by an order of magnitude.

In this study, we have found that a super-massive star is likely to shed most of its mass well before it experiences a supernova explosion. In several cases the supernova progenitor still had  $\gtrsim 100 M_\odot$ , and such objects could possibly collapse to black holes of intermediate mass but with  $M_{bh} \ll 1000 M_\odot$ . Our calculations suggest the possibility of the formation of objects that experience pair-instability supernovae, which would be interesting phenomena to observe. The recently discovered, very luminous supernova 2006gy may have been a PISN (Smith et al. 2007; Ofek et al. 2007; Langer et al. 2007), although this is still under debate.

Obviously there is the possible caveat that the quantitative difference between starting as a homogeneous high-mass star (as we considered in our paper), or growing to one over the main-sequence lifetime by repeated collisions may be significant, but at this stage we cannot provide further insights about the consequences of these potential differences. We therefore draw our conclusions on the calculations at hand, and we argue that the majority of supermassive stars probably end up as black holes of  $M \lesssim 70 M_\odot$ , with the possible exception of some of them exploding as pair-instability supernovae. With the

approximate nature of our applied mass-loss algorithm in mind, and also taking into account the (also approximate) results of Belkus et al. (2007), we infer that the accuracy on the limit for black hole masses is  $\sim \pm 30 M_\odot$ . We therefore conclude that most supermassive stars end their lives as  $70 \pm 30 M_\odot$  black holes.

## Acknowledgments

We thank the referee, A. Maeder, for constructive comments that helped improve the paper. We also thank L. Kaper, G.-J. Savonije, N. Langer, Yu. Fadeyev, N. Chugai, D. Vanbeveren and O. Pols for productive discussions. LRY acknowledges P.P. Eggleton for providing his evolutionary code and advice on its usage. Z. Han is acknowledged for sharing his knowledge of this code. We thank F. Martins and G. Rauw for providing us the data in advance of publication. LRY is supported by NWO (via grants #635.000.303 and #643.200.503), NOVA, the Russian Academy of Sciences Basic Research Program “Origin and Evolution of Stars and Galaxies” and the Russian Foundation for Basic Research grant #07-02-00454. LRY acknowledges warm hospitality and support from the Astronomical Institute “Anton Pannekoek”, where most part of this study was carried out.

## APPENDIX: Notes on individual stars

We first discuss the enigmatic LBV  $\eta$  Car. We adopt a luminosity of  $5 \times 10^6 L_\odot$ , which corresponds to the observed IR-flux and assumed distance of 2.3 Kpc (Hillier et al. 2001). The positions of the two labels for the star in the HR-diagram reflect the ambiguity in the determination of the stellar radius, caused by the presence of an optically thick wind that dominates the spectrum and prevents the determination of  $R_\star$ . The maximum and minimum  $T_{\text{eff}}$  correspond to a Rosseland optical depth of  $\tau = 155$  and 0.67 respectively in the atmosphere.  $\eta$  Car may be a  $2020 \pm 5$  day binary (Damineli et al. 1997, 2000). Assuming that the luminosity is Eddington, Hillier et al. (2001) estimate the minimum total mass of the system to be  $150[L/(5 \times 10^6)] M_\odot$ , but some contribution of the secondary star is probably not very significant, although the secondary is possibly a late-O/WR star (Iping et al. 2005). Our computations show that the luminosity of a several hundred solar mass star may still be far from the Eddington limit. The estimated mass-loss rate is  $\dot{M} \approx 10^{-3} M_\odot \text{ yr}^{-1}$ . Bearing in mind that  $M_0 = (200 - 300) M_\odot$  stars in their core-hydrogen burning stage evolve at almost constant luminosity,  $L = 5 \times 10^6 L_\odot$  in our computations corresponds to a ZAMS mass of about  $250 M_\odot$ . Hillier et al. (2001) derive for the  $\eta$  Car atmosphere a H/He fraction of  $\approx 5$  by number, i.e.  $X \approx 0.56$ ,  $Y \approx 0.44$ . Thus,  $L$ ,  $X$ ,  $Y$ ,  $\dot{M}$ , and the “high”  $T_{\text{eff}}$  solution suggest that  $\eta$  Car is a  $\sim 250 M_\odot$  star somewhere in the middle of the core-hydrogen burning stage. The nature of its instability has yet to be found.

<sup>7</sup> These results were obtained using standard models for run-away mass accumulation without accounting for the possibility of vigorous mass loss as considered in the present paper.

The position of the candidate LBV Pistol star is drawn according to the “low-luminosity” solution of Figer et al. (1998), since Najarro et al. (1999) found that its metal content equals  $Z \simeq 3Z_{\odot}$ , corresponding to its location in the star-forming region of the Galactic center, and that this favours the lower luminosity solution for its stellar parameters. Note however that, if it turns out that the Pistol star is an LBV, its  $T_{\text{eff}}$  will be variable. Of all our tracks, the one for  $M_0 = 200 M_{\odot}$  seems to provide the best fit of the position of the Pistol star. Figer et al. (1998) find  $Y=0.3-0.4$  at the surface of the Pistol star, as well as strong N enhancement. Going redward, at  $\log T_{\text{eff}} = 4.15$ , our  $M_0 = 200 M_{\odot}$  evolutionary sequence has a mass  $M = 92 M_{\odot}$  and  $Y=0.86$ . Going blueward, it has a mass of  $M=86.5 M_{\odot}$  and  $Y=0.91$ . We therefore cannot match the chemical composition of the Pistol star. Other tracks passing through the same position also have too high a helium fraction  $Y$ . For instance, the track for  $M_0 = 120 M_{\odot}$ , which runs slightly lower than the error box of the Pistol star, has  $Y > 0.7$ . Note that the determination of the He-abundance is challenging. However, if the high metallicity of the Pistol star is real, it may be an almost unevolved star: Ishii et al. (1999, see their Fig. 6) find that the Pistol star lies very close to the ZAMS for stars with  $X=0.7$ ,  $Z=0.1$ ; its mass is then slightly higher than  $200 M_{\odot}$ <sup>8</sup>.

There is another LBV star in the Quintuplet cluster, similar to the Pistol star: FMM362 (Figer et al. 1999; Geballe et al. 2000). The latter authors report  $T_{\text{eff}} = (10000 - 13000) \text{ K}$  for this object, with  $L \geq 10^6 L_{\odot}$ .

For the stars in the HeI cluster in the Galactic centre, we show  $\dot{M}$  estimates from Martins et al. (2007). The positions of the HeI stars in the HR-diagram are consistent with their interpretation as being evolved blue supergiants, close to the WR stage. We note that the evolutionary stage of the HeI star has to be very short.

We note that the WN stars – termed AdK – may be in their core-hydrogen burning stage, as they are positioned along portions of the tracks where  $Y$  is only moderately enhanced.

The cool hypergiant IRC +10 420 is the only object that is believed to be observed in the phase of rapid transition from the red supergiant stage to the WR phase (see e.g. Humphreys et al. 1997; Blöcker et al. 1999, and references therein). Its  $T_{\text{eff}}$  appears to have increased by 1000 – 2000 K within the last 20 years. We note that Smith et al. (2004) computed radiation-driven wind models for objects with a low stellar mass and discussed the possibility that these cool hypergiants like IRC +10 420 may in fact be “LBVs in disguise”, where a large mass-loss rate induced by the high Eddington factor produces a pseudo-photosphere. Although the object is located in the HR-diagram at the lowest luminosity level, based on our calculations we expect the existence of similar more luminous stars, which have to be extremely rare due to

their short lifetimes.  $\rho$  Cas may be an example of star that is in an unstable post-RSG stage of evolution, when it experiences outbursts ejecting mass at a rate of several  $0.01 M_{\odot} \text{ yr}^{-1}$  (Lobel et al. 2003).

We show the position of one of the brighter LBVs, AG Car, after Humphreys & Davidson (1994) and Lamers et al. (1996a). Two data labels illustrate the range of excursions over the HR-diagram experienced by the LBV.

Especially remarkable is WR20a, a  $P_{\text{orb}} \approx 3.68$  day massive binary (Rauw et al. 2004, 2005; Bonanos et al. 2004) with both components of a WN6ha spectral type (see Fig. 11). The component mass estimates are  $83 \pm 5.0 M_{\odot}$  and  $82 \pm 5.0 M_{\odot}$  (Bonanos et al. 2004). This makes these components of WR20a the most massive stars weighed in binaries. According to Rauw et al. (2005), fundamental parameters of each of the components are:  $T_{\text{eff}} = 43000 \pm 2000 \text{ K}$ ,  $L_{\text{bol}}/L_{\odot} \simeq (1.15 \pm 0.15) \times 10^6$ ,  $\dot{M} = 8.5 \times 10^{-6} M_{\odot} \text{ yr}^{-1}$  (assuming a clumped wind with a volume filling factor  $f = 0.1$ ). Nitrogen is enhanced in the atmospheres, whilst carbon is depleted. Spectral classification implies only a weak helium enrichment of the atmosphere. The origin and evolution of this system deserves urgent study. Rauw et al. (2005) propose that the position of the WR20a components in the HR-diagram “suggests that they are core hydrogen burning stars in a pre-LBV stage and their current atmospheric chemical composition probably results from rotational mixing that might be enhanced in a close binary compared to a single star of the same age”. However, we should note that the evolution with complete mixing of a high-rotational velocity star in a synchronised binary with mass loss may result in evolutionary tracks that evolve to the left of the ZAMS, in apparent conflict with the position of WR20a. As Figs. 10 and 11 show,  $T_{\text{eff}}$ ,  $L$ , and  $\dot{M}$  of WR20a are actually quite consistent with a star with an initial mass of about  $100 M_{\odot}$  in a rather early stage of core-hydrogen burning, when the layers enriched in He are beginning to be exposed.

In addition to the Galactic stars, we plot some Magellanic Clouds stars in Fig. 11. Most remarkable are the R136 cluster members of O3(If\*) and O3If\*/WN6A subtypes that are considered to be transitional between O and WN type stars (Massey & Hunter 1998)<sup>9</sup>. The stars are located along the ZAMS or slightly to the left of it. The R136 cluster belongs to the LMC and has a several times lower  $Z$  than Galactic stars. Figure 6 of Ishii et al. (1999) shows that in the  $(100-200) M_{\odot}$  range, ZAMS stars with  $Z=0.004$  are  $\sim 0.1$  dex in  $\log T_{\text{eff}}$  hotter than  $Z=0.02$  stars, but they have the same luminosity. As our Fig. 11 shows,  $(100-200) M_{\odot}$  stars may easily reveal over-abundances of helium, whilst they evolve over  $\Delta \log T_{\text{eff}} \sim 0.1$  in the HR-diagram. The surface helium

<sup>8</sup> We must note however that the models of Ishii et al. (1999) for mass higher than  $\simeq 200 M_{\odot}$  have more extended envelopes than our models.

<sup>9</sup> The degeneracy with respect to the effective temperature is caused by the absence of individual determinations of  $T_{\text{eff}}$ . The latter were assigned according to spectral type after Vacca et al. (1996).

abundance increases to  $Y = 0.4$  in  $\sim 0.5$  Myr. Therefore, R136 cluster members may be very massive stars that are still in their core H-burning phase, with a strong stellar wind that causes the spectrum to mimic that of evolved WR stars, as was originally conjectured for one of these stars (R136-006 $\equiv$ R136a3) by de Koter et al. (1997). Another possibility is that the surface layers enriched in helium are already exposed (this may happen in  $\sim 1$  Myr, see Fig. 5). This is also consistent with the star formation history of R136 (see the discussion in Massey & Hunter 1998). We also note that the effective-temperature scale by Martins et al. (2005) assigns O3I-type stars  $\log T_{eff} \approx 4.6$  (instead of 4.7 in Vacca et al. 1996) and smaller bolometric corrections (implying a reduction of the luminosity by  $\approx 0.25$  dex). This would move these stars to the right of the ZAMS, in the proper direction. The position of R136 members in the HR-diagram is roughly consistent with the estimate of the upper limit of masses of stars in this complex of  $(140\text{--}160) M_{\odot}$  obtained by Koen (2006) by power-law distribution fitting to these stars.

Finally, we also plot P Cygni (Lamers et al. 1996b) in Figs. 11 and 12, and show the positions of several other high-luminosity Galactic stars for which our calculations may be relevant (see Table 2 to identify them if they are not annotated in the Figures).

## References

- Aerts, C., Lamers, H. J. G. L. M., & Molenberghs, G. 2004, *A&A*, 418, 639
- Alexander, D. R. & Ferguson, J. W. 1994, *ApJ*, 437, 879
- Appenzeller, I. 1970, *A&A*, 9, 216
- Baraffe, I., Heger, A., & Woosley, S. E. 2001, *ApJ*, 550, 890
- Baumgardt, H., Hut, P., Makino, J., McMillan, S., & Portegies Zwart, S. 2003a, *ApJ*, 582, L21
- Baumgardt, H., Makino, J., Hut, P., McMillan, S., & Portegies Zwart, S. 2003b, *ApJ*, 589, L25
- Behrend, R. & Maeder, A. 2001, *A&A*, 373, 190
- Belkus, H., Van Bever, J., & Vanbeveren, D. 2007, *ApJ*, 659, 1576
- Blöcker, T., Balega, Y., Hofmann, K.-H., et al. 1999, *A&A*, 348, 805
- Bonanos, A. Z., Stanek, K. Z., Udalski, A., et al. 2004, *ApJ*, 611, L33
- Cappa, C., Goss, W. M., & van der Hucht, K. A. 2004, *AJ*, 127, 2885
- Caughlan, G. R. & Fowler, W. A. 1988, *Atomic Data and Nuclear Data Tables*, 40, 283
- Caughlan, G. R., Fowler, W. A., Harris, M. J., & Zimmerman, B. A. 1985, *Atomic Data and Nuclear Data Tables*, 32, 197
- Colbert, E. J. M. & Miller, M. C. 2005, in *The Tenth Marcel Grossmann Meeting. On recent developments in theoretical and experimental general relativity, gravitation and relativistic field theories*, ed. M. Novello, S. Perez Bergliaffa, & R. Ruffini, 530–549
- Crowther, P. A., Lennon, D. J., & Walborn, N. R. 2006, *A&A*, 446, 279
- Damineli, A., Conti, P. S., & Lopes, D. F. 1997, *New Astronomy*, 2, 107
- Damineli, A., Kaufer, A., Wolf, B., et al. 2000, *ApJ*, 528, L101
- de Donder, E. & Vanbeveren, D. 2003, *New Astronomy*, 8, 415
- de Jager, C. 1998, *A&A Rev.*, 8, 145
- de Jager, C., Nieuwenhuijzen, H., & van der Hucht, K. A. 1988, *Astron. and Astrophys. Suppl.*, 72, 259
- de Koter, A., Heap, S. R., & Hubeny, I. 1997, *ApJ*, 477, 792
- De Rijcke, S., Buyle, P., & Dejonghe, H. 2006, *MNRAS*, 368, L43
- DePoy, D. L., Pepper, J., Pogge, R. W., et al. 2004, *ApJ*, 617, 1127
- Eggleton, P. P. 1971, *MNRAS*, 151, 351
- Fabbiano, G. 1989, *ARA&A*, 27, 87
- Fabbiano, G. 2006, *ARA&A*, 44, 323
- Fabbiano, G. & White, N. E. 2006, *Compact stellar X-ray sources in normal galaxies (Compact stellar X-ray sources)*, 475–506
- Fadeyev, Y. A. & Novikova, M. F. 2004, *Astronomy Letters*, 30, 707
- Feng, H. & Kaaret, P. 2006, *ApJ*, 653, 536
- Figer, D. F. 2005, *Nature*, 434, 192

- Figer, D. F., Kim, S. S., Morris, M., et al. 1999, *ApJ*, 525, 750
- Figer, D. F., Najarro, F., Morris, M., et al. 1998, *ApJ*, 506, 384
- Fraley, G. S. 1968, *Ap&SS*, 2, 96
- Freitag, M., Gürkan, M. A., & Rasio, F. A. 2006, *MNRAS*, 368, 141
- Fryer, C. L. 1999, *ApJ*, 522, 413
- Fryer, C. L. & Kalogera, V. 2001, *ApJ*, 554, 548
- Geballe, T. R., Najarro, F., & Figer, D. F. 2000, *ApJ*, 530, L97
- Gebhardt, K., Rich, R. M., & Ho, L. C. 2005, *ApJ*, 634, 1093
- Gerssen, J., van der Marel, R. P., Gebhardt, K., et al. 2002, *AJ*, 124, 3270
- Gerssen, J., van der Marel, R. P., Gebhardt, K., et al. 2003, *AJ*, 125, 376
- Gürkan, M. A., Freitag, M., & Rasio, F. A. 2004, *ApJ*, 604, 632
- Hamann, W.-R., Gräfener, G., & Liermann, A. 2006, *A&A*, 457, 1015
- Hamann, W.-R. & Koesterke, L. 1998, *A&A*, 335, 1003
- Heger, A. & Woosley, S. E. 2002, *ApJ*, 567, 532
- Hillier, D. J., Davidson, K., Ishibashi, K., & Gull, T. 2001, *ApJ*, 553, 837
- Hubbard, W. B. & Lampe, M. 1969, *ApJS*, 18, 297
- Humphreys, R. M. & Davidson, K. 1994, *PASP*, 106, 1025
- Humphreys, R. M., Smith, N., Davidson, K., et al. 1997, *AJ*, 114, 2778
- Iglesias, C. A. & Rogers, F. J. 1996, *ApJ*, 464, 943
- Iping, R. C., Sonneborn, G., Gull, T. R., Massa, D. L., & Hillier, D. J. 2005, *ApJ*, 633, L37
- Ishii, M., Ueno, M., & Kato, M. 1999, *PASJ*, 51, 417
- Itoh, N., Mitake, S., Iyetomi, H., & Ichimaru, S. 1983, *ApJ*, 273, 774
- Kaaret, P., Prestwich, A. H., Zezas, A., et al. 2001, *MNRAS*, 321, L29
- Kato, M. 1985, *PASJ*, 37, 311
- Kato, M. 1986, *Ap&SS*, 119, 57
- Koen, C. 2006, *MNRAS*, 365, 590
- Koenigsberger, G. 2004, *Revista Mexicana de Astronomia y Astrofisica*, 40, 107
- Kudritzki, R. P. 2002, *ApJ*, 577, 389
- Kudritzki, R.-P. & Puls, J. 2000, *ARA&A*, 38, 613
- Lamers, H. J. G. L. M., Morris, P. W., Voors, R. H. M., et al. 1996a, *A&A*, 315, L225
- Lamers, H. J. G. L. M., Najarro, F., Kudritzki, R. P., et al. 1996b, *A&A*, 315, L229
- Lang, C. C., Johnson, K. E., Goss, W. M., & Rodríguez, L. F. 2005, *AJ*, 130, 2185
- Langer, N. 1989, *A&A*, 220, 135
- Langer, N. 1997, in *ASP Conf. Ser. 120: Luminous Blue Variables: Massive Stars in Transition*, 83
- Langer, N., Norman, C. A., de Koter, A., et al. 2007, *A&A*
- Lennon, D. J., Wobig, D., Kudritzki, R. P., & Stahl, O. 1993, *Space Science Reviews*, 66, 207
- Levesque, E. M., Massey, P., Olsen, K. A. G., et al. 2005, *ApJ*, 628, 973
- Limongi, M. & Chieffi, A. 2007, in *American Institute of Physics Conference Series*, Vol. 924, American Institute of Physics Conference Series, 226–233
- Lobel, A., Dupree, A. K., Stefanik, R. P., et al. 2003, *ApJ*, 583, 923
- Lu, J. R., Ghez, A. M., Hornstein, S. D., Morris, M., & Becklin, E. E. 2004, *American Astronomical Society Meeting Abstracts*, 205
- Maeder, A. 1980, *A&A*, 92, 101
- Maeder, A. 1992, *A&A*, 103, 97
- Maillard, J. P., Paumard, T., Stolovy, S. R., & Rigaut, F. 2004, *A&A*, 423, 155
- Marchenko, S. V., Foellmi, C., Moffat, A. F. J., et al. 2007, *ApJ*, 656, L77
- Martins, F., Genzel, R., Hillier, D. J., et al. 2007, *A&A*, 468, 233
- Martins, F., Schaerer, D., & Hillier, D. J. 2005, *A&A*, 436, 1049
- Martins, F., Trippe, S., Paumard, T., et al. 2006, *ApJ*, 649, L103
- Massey, P. & Hunter, D. A. 1998, *ApJ*, 493, 180
- Massey, P., Parker, J. W., & Garmany, C. D. 1989, *AJ*, 98, 1305
- Massey, P., Puls, J., Pauldrach, A. W. A., et al. 2005, *ApJ*, 627, 477
- Matsumoto, H., Tsuru, T. G., Koyama, K., et al. 2001, *ApJ*, 547, L25
- Mayya, Y. D., Bressan, A., Carrasco, L., & Hernandez-Martinez, L. 2006, *ApJ*, 649, 172
- McLeod, K. K., Rieke, G. H., Rieke, M. J., & Kelly, D. M. 1993, *ApJ*, 412, 111
- McMillan, S., Baumgardt, H., Portegies Zwart, S., Hut, P., & Makino, J. 2004, in *ASP Conf. Ser. 322: The Formation and Evolution of Massive Young Star Clusters*, 449
- Menshchikov, A. B. & Tutukov, A. V. 1989, *Astrophysics*, 29, 714
- Miller, M. C. & Colbert, E. J. M. 2004, *International Journal of Modern Physics D*, 13, 1
- Miller, M. C. & Hamilton, D. P. 2002, *MNRAS*, 330, 232
- Najarro, F., Figer, D. F., Hillier, D. J., & Kudritzki, R. P. 2004, *ApJ*, 611, L105
- Najarro, F., Hillier, D. J., Figer, D. F., & Geballe, T. R. 1999, in *ASP Conf. Ser. 186: The Central Parsecs of the Galaxy*, 340
- Najarro, F., Krabbe, A., Genzel, R., et al. 1997, *A&A*, 325, 700
- Nelemans, G. & van den Heuvel, E. P. J. 2001, *A&A*, 376, 950
- Nieuwenhuijzen, H. & de Jager, C. 2000, *A&A*, 353, 163
- Nugis, T. & Lamers, H. J. G. L. M. 2000, *A&A*, 360, 227
- Ober, W. W., El Eid, M. F., & Fricke, K. J. 1983, *A&A*, 119, 61
- Ofek, E. O., Cameron, P. B., Kasliwal, M. M., Gal-Yam, A., & Rau, A. 2007, *ApJ*, 659, 13
- Okajima, T., Ebisawa, K., & Kawaguchi, T. 2006, *ApJ*, 652, L105

- Origlia, L., Ranalli, P., Comastri, A., & Maiolino, R. 2004, *ApJ*, 606, 862
- Papaloizou, J. C. B. 1973, *MNRAS*, 162, 169
- Patruno, A., Portegies Zwart, S., Dewi, J., & Hopman, C. 2006, *MNRAS*, 370, L6
- Peeples, M. S., Bonanos, A. Z., DePoy, D. L., et al. 2007, *ApJ*, 654, L61
- Pols, O. R., Tout, C. A., Eggleton, P. P., & Han, Z. 1995, *MNRAS*, 274, 964
- Portegies Zwart, S. 2004, *ArXiv Astrophysics e-prints*, astro-ph/0410531
- Portegies Zwart, S. F., Baumgardt, H., Hut, P., Makino, J., & McMillan, S. L. W. 2004, *Nature*, 428, 724
- Portegies Zwart, S. F., Baumgardt, H., McMillan, S. L. W., et al. 2006, *ApJ*, 641, 319
- Portegies Zwart, S. F., Makino, J., McMillan, S. L. W., & Hut, P. 1999, *A&A*, 348, 117
- Portegies Zwart, S. F. & McMillan, S. L. W. 2002, *ApJ*, 576, 899
- Ptak, A. & Griffiths, R. 1999, *ApJ*, 517, L85
- Rakavy, G. & Shaviv, G. 1967, *ApJ*, 148, 803
- Rauw, G., Crowther, P. A., de Becker, M., et al. 2005, *A&A*, 432, 985
- Rauw, G., De Becker, M., Nazé, Y., et al. 2004, *A&A*, 420, L9
- Repolust, T., Puls, J., & Herrero, A. 2004, *A&A*, 415, 349
- Schaller, G., Schaerer, D., Meynet, G., & Maeder, A. 1992, *Astron. and. Astrophys. Suppl.*, 96, 269
- Schödel, R., Eckart, A., Iserlohe, C., Genzel, R., & Ott, T. 2005, *ApJ*, 625, L111
- Smith, L. J., Nota, A., Pasquali, A., et al. 1998, *ApJ*, 503, 278
- Smith, N., Li, W., Foley, R. J., et al. 2007, *ApJ*, 666, 1116
- Smith, N. & Owocki, S. P. 2006, *ApJ*, 645, L45
- Smith, N., Vink, J. S., & de Koter, A. 2004, *ApJ*, 615, 475
- Soria, R. 2006, *ArXiv Astrophysics e-prints*, astro-ph/0611152
- Stothers, R. B. & Chin, C.-W. 1999, *ApJ*, 522, 960
- Strohmayer, T. E. & Mushotzky, R. F. 2003, *ApJ*, 586, L61
- Suzuki, T., Nakasato, N., & Baumgardt, H. 2007, *ApJ*
- Umeda, H. & Nomoto, K. 2002, *ApJ*, 565, 385
- Vacca, W. D., Garmany, C. D., & Shull, J. M. 1996, *ApJ*, 460, 914
- Vanbeveren, D. 2005, in *AIP Conf. Proc. 797: Interacting Binaries: Accretion, Evolution, and Outcomes*, ed. L. Burderi, L. A. Antonelli, F. D'Antona, T. di Salvo, G. L. Israel, L. Piersanti, A. Tornambè, & O. Straniero, 445–452
- Vink, J. S. 2006, in *ASP Conf. Ser. 353: Stellar Evolution at Low Metallicity: Mass Loss, Explosions, Cosmology*, ed. H. J. G. L. M. Lamers, N. Langer, T. Nugis, & K. Annuk, 113
- Vink, J. S., de Koter, A., & Lamers, H. J. G. L. M. 2000, *A&A*, 362, 295
- Vink, J. S., de Koter, A., & Lamers, H. J. G. L. M. 2001, *A&A*, 369, 574
- Walborn, N. R. & Blades, J. C. 1997, *ApJS*, 112, 457
- Waldron, W. L., Cassinelli, J. P., Miller, N. A., MacFarlane, J. J., & Reiter, J. C. 2004, *ApJ*, 616, 542
- Weidner, C. & Kroupa, P. 2004, *MNRAS*, 348, 187

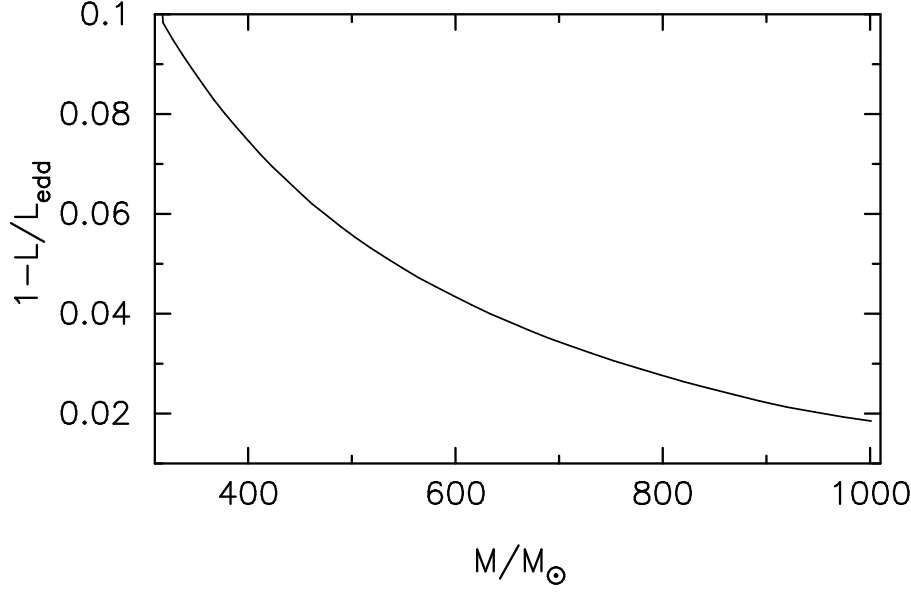
**Table 1.** Summary of calculated evolutionary tracks. Successive columns give the initial mass  $M_0$ , the value of the  $\alpha$  parameter, the age at the terminal age main-sequence  $t_{\text{TAMS}}$ , the mass at the TAMS  $M_{\text{TAMS}}$ , the age of the last computed model  $t_f$ , the mass of the last computed model  $M_f$ , the central abundances of He, C, and O in the last model  $Y_{\text{cf}}$ ,  $X_{\text{C,cf}}$ ,  $X_{\text{O,cf}}$ , and the abundances of H and He at the surface of the last computed model  $X_{\text{sf}}$ ,  $Y_{\text{sf}}$ . Note that helium burning results in the formation of oxygen-neon cores with traces of carbon. The “V” in the second column stands for the  $60 M_{\odot}$  track computed using the mass-loss prescription of Vink et al. (2000).

$M_0$	$\alpha$	$t_{\text{TAMS}}, 10^6 \text{ yr}$	$M_{\text{TAMS}}$	$t_f, 10^6 \text{ yr}$	$M_f$	$Y_{\text{cf}}$	$X_{\text{C,cf}}$	$X_{\text{O,cf}}$	$X_{\text{sf}}$	$Y_{\text{sf}}$
1001	1.0	2.492	29.66	2.594	25.24	0.648	0.287	0.039	0.0	0.976
1001	0.9	2.360	34.82	2.713	20.25	0.018	0.141	0.811	0.0	0.204
1001	0.8	2.244	41.46	2.541	25.11	0.082	0.262	0.630	0.0	0.286
1001	0.5	1.935	86.81	2.218	49.17	0.0035	0.061	0.856	0.0	0.174
1001	0.3	1.792	219.9	1.793	218.4	0.981	0.00028	0.00022	0.025	0.958
1001	0.25	1.777	229.0	2.019	139.6	$9.4 \cdot 10^{-4}$	0.0	0.819	0.035	0.200
844	1.0	2.513	29.56	2.899	13.61	0.0	0.115	0.844	0.0	0.030
598	1.0	2.572	29.20	2.591	27.91	0.953	0.021	0.0004	0.038	0.943
500	1.0	2.605	28.96	2.623	26.96	0.948	0.024	0.00045	0.033	0.948
500	0.9	2.483	33.91	2.837	20.09	0.019	0.145	0.806	0.0	0.213
500	0.8	2.372	40.02	2.696	23.86	0.046	0.195	0.731	0.040	0.239
500	0.5	2.104	75.76	2.393	46.95	0.0	0.062	0.852	0.0	0.195
500	0.3	1.981	163.7	1.982	163.3	0.981	0.00045	0.00023	0.057	0.923
500	0.25	1.956	183.4	2.206	115.1	$0.41 \cdot 10^{-3}$	0.0	0.827	0.039	0.215
200	1.0	2.951	26.76	2.997	25.74	0.960	0.014	0.00032	0.051	0.930
200	0.9	2.837	30.75	3.208	18.98	0.010	0.128	0.828	0.0	0.228
200	0.8	2.740	35.51	3.083	22.31	0.027	0.157	0.786	0.0	0.238
200	0.5	2.511	56.71	2.525	54.61	0.981	0.0004	0.00024	0.047	0.934
200	0.3	2.379	81.92	2.397	76.12	0.980	0.0004	0.00024	0.073	0.907
200	0.25	2.350	92.28	2.629	61.88	0.0	0.00556	0.846	0.0	0.304
120	1.0	3.345	24.15	3.360	23.67	0.974	0.0012	0.00027	0.074	0.398
120	0.5	2.906	44.36	2.915	44.19	0.975	0.00070	0.00025	0.094	0.887
120	0.4	2.836	50.74	2.844	50.52	0.980	0.00037	0.00025	0.133	0.848
120	0.35	2.813	54.41	3.108	37.86	0.981	0.00036	0.00025	0.163	0.818
120	0.3	2.771	58.79	3.080	39.34	0.847	0.073	0.847	0.0	0.320
120	0.25	2.786	63.02	3.077	40.38	0.043	0.146	0.781	0.0	0.427
120	0.10	2.900	47.64	3.007	44.48	0.010	0.077	0.851	0.077	0.548
60	0.5	3.394	29.56	4.357	18.34	0.0	0.123	0.834	0.0	0.975
60	0.25	3.807	36.31	4.213	20.94	0.0	0.113	0.834	0.0	0.978
60	V	3.685	40.60	3.787	26.20	0.719	0.228	0.023	0.0	0.876

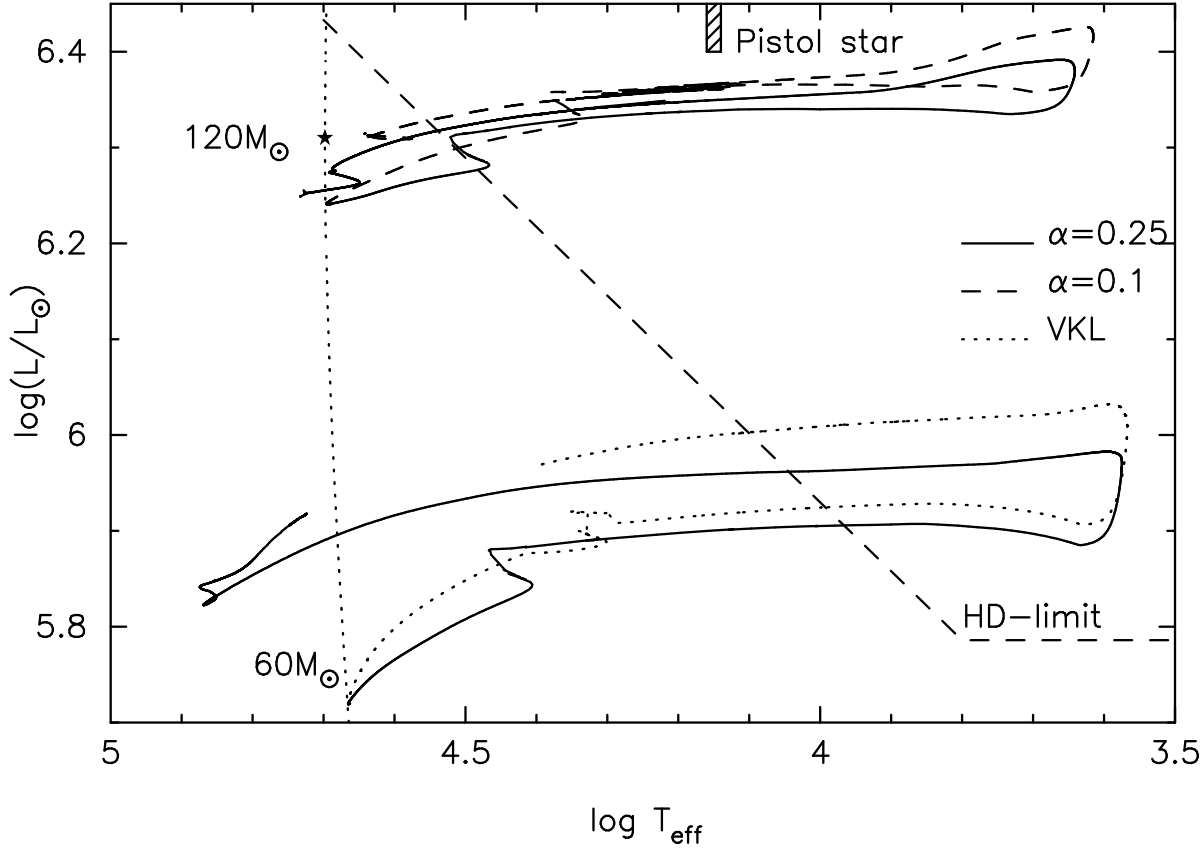
**Table 2.** Some of the most luminous stars in the Galaxy and Magellanic Clouds.

No.	Star	Sp. type	$\log L/L_{\odot}$	$\log T_{\text{eff}}$	$M, 10^{-6} M_{\odot} \text{ yr}^{-1}$	$M/M_{\odot}$	Ref.	Comment
1	HD5280A	LBV	6.5	4.724		50.	1	SMC, Y/X=0.63
2	HD5280B	WNE?	6.3	4.748		28.	1	Comp. to A., X=0
3	HD5280C	O4-6	6.1	4.665			1	N enhanced
4	Sk 80	O7If	6.1	4.560			2	SMC
5	MPG355	ON3III(f*),	6.98	4.690			2	SMC
6	R136-040	O2-3.5 V	5.82	4.71	2.0	25.	3	LMC
7	BI 253	O2 V((f*))	5.82	4.68	3.5	43.	3	...
8	BI 237	O2 V((f*))	5.77	4.68	2.0	37.	3	...
9	AV 435	O3 V((f*))	5.87	4.653	0.5	48.	3	SMC
10	AV 14	O5 V	5.85	4.643	0.3	75.	3	SMC
11	LH64-16	ON2 III(f*)	5.85	4.74	4.0	26.	3	LMC
12	R136-047	O2 III(f*)	5.82	4.71	6.0	32.	3	...
13	R136-018	O3 III(f*)	5.9	4.65	2.0	46.	3	...
14	LH90:ST2-22	O3.5 III(f+)	6.08	4.643	4.5	67.	3	...
15	LH101:W3-19	O2 If*	6.34	4.643	20.	193.	3	...
16	R136-036	O2 If*	5.7	4.633	14.	31.	3	...
17	R136-020	O2 If*	5.9	4.628	23.	40.	3	...
18	Sk -67 22	O2 If*	5.69	4.623	15.	23.	3	...
19	LH90:Br58	O3If/WN6	5.9	4.613	40.	40.	3	...
20	R136-014	O3.5 If*	5.9	4.58	23.	53.	3	...
21	Sk -65 47	O4 If	5.97	4.60	12.	61.	3	...
22	AV 75	O5.5 I(f)	6.16	4.60	3.5	96.	3	SMC
23	AV 26	O6 I(f)	6.14	4.58	2.5	91.	3	...
24	HD93250	O3 V ((f))	6.01	4.662	3.45	83.3	4	...
25	HD66811	O4 I(f)	5.90	4.613	8.8	53.9	4	...
26	HD14947	O5 If+	5.90	4.574	8.52	30.7	4	...
27	HD15558	O5 III(f)	5.93	4.613	5.58	78.7	4	...
28	HD210839	O6 I(n) fp	5.83	4.556	6.85	62.2	4	...
29	HD30614	O9.5 Ia	5.83	4.462	6.04	37.6	4	...
30	KY Cyg	M3-4 I	5.43 - 6.04	3.544			5	MW
31	BD+60 2613	M3 I	5.32 - 5.75	3.544			5	...
32	Mk51	O3If/WN7-A	6.23	4.648			6	LMC
33	R139	O7Iafp	6.40	4.558			6	...
34	Mk26	O4 III(f)	6.02	4.647			6	...
35	Mk24	O3V	6.00	4.686			6	...
36	Mk14	O3-6V	5.94	4.646			6	...
37	IRC+10420	OH/IR	5.7	3.845	300-600		7	MW
38	CygOB2 No.9	O5f	6.6	4.650	12.7	160.	8	...
39	CygOB2 No.8A	O5.5 I(f)	6.18	4.585	13.5	118.	8	...
40	CygOB2 No.12	B8 Ia	6.20	4.049	38.5	71.	8	...
41	HD 33579	A3 Ia <sup>+</sup>	5.72	3.902	2.	20.-30.	9	LMC
42	HD80077	B2 Ia <sup>+</sup>	6.4	4.23			10	MW, (LBV?)
43	HD119796	G8 Ia <sup>+</sup>	5.7	3.67			10	...
44	HD152234	B05 Ia(N wk)	5.87	4.41	2.7		11	...
45	HD15236	B1.5 Ia	6.1	4.26	6.0		11	...
46	HD224914 ( $\rho$ Cas)	F8 Ia <sup>+</sup>	5.70	3.86	54000.		11, 12	..., $\dot{M}$ in outburst

References: 1 – Koenigsberger (2004), 2 – Massey et al. (1989), 3 – Massey et al. (2005), 4 – Repolust et al. (2004), 5 – Levesque et al. (2005), 6 – Walborn & Blades (1997), 7 – Humphreys et al. (1997), 8 – Waldron et al. (2004), 9 – Nieuwenhuijzen & de Jager (2000), 10 – de Jager (1998), 11 – Crowther et al. (2006), 12 – Lobel et al. (2003)

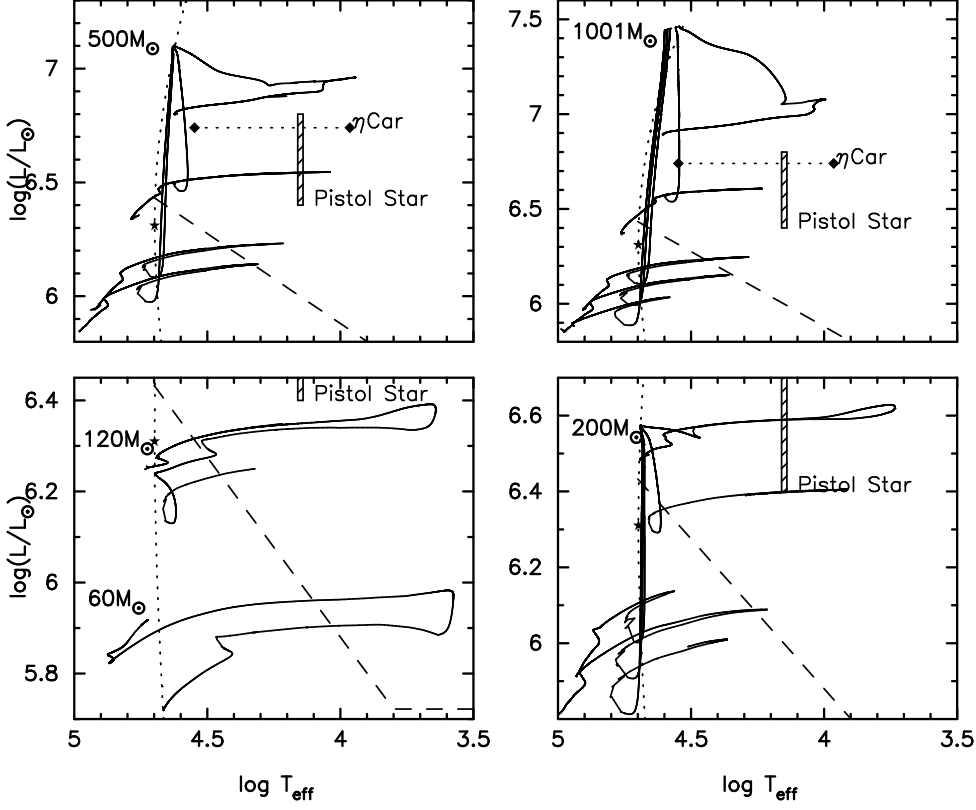


**Fig. 1.** The behaviour of the factor  $\Gamma = 1 - L/L_{\text{Edd}}$  in the outermost meshpoint of the models along the sequence of homogeneous models.

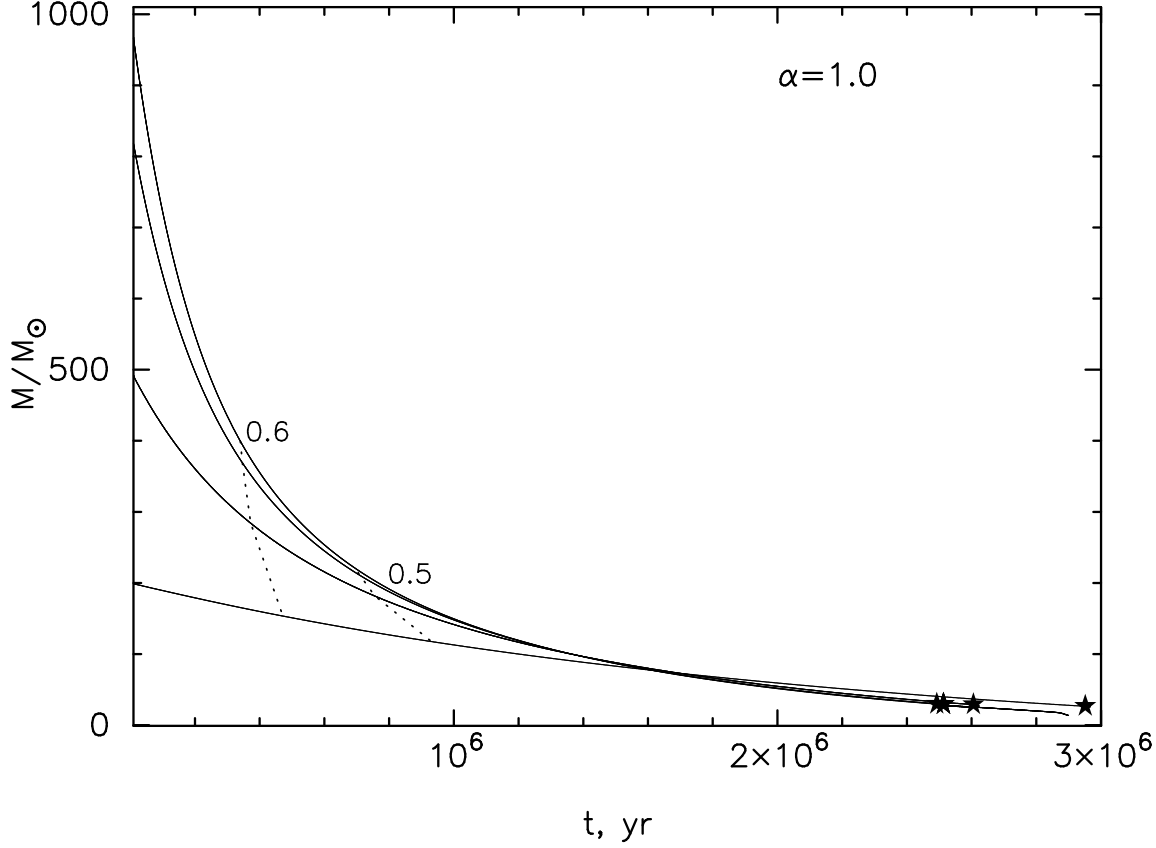


**Fig. 2.** Evolutionary tracks of stars with  $M_0=60$  and  $120M_\odot$  in the Hertzsprung-Russell diagram for different assumptions of the mass-loss prescription. For  $60 M_\odot$ , the tracks for mass-loss prescription given by Eq. (4) with  $\alpha=0.25$  and mass-loss rates from Vink et al. (2000) are shown. For  $120 M_\odot$ , tracks for Eq. (4) prescription with  $\alpha=0.25$  and  $0.1$  are shown. The long-dashed broken line shows the Humphreys-Davidson limit. The star symbol marks the bending of the sequence of homogeneous models.

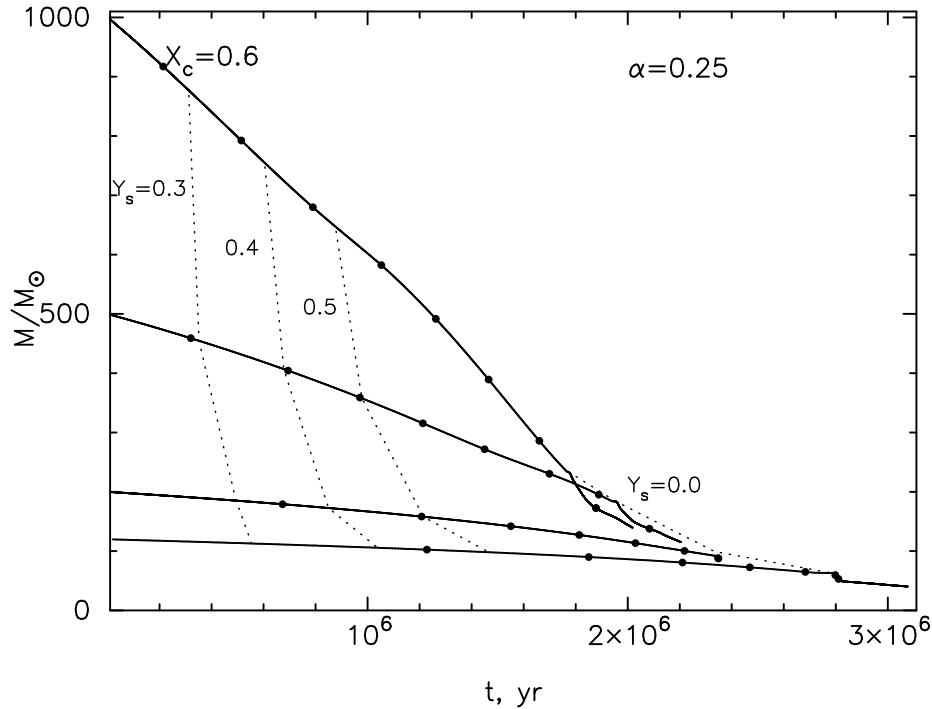




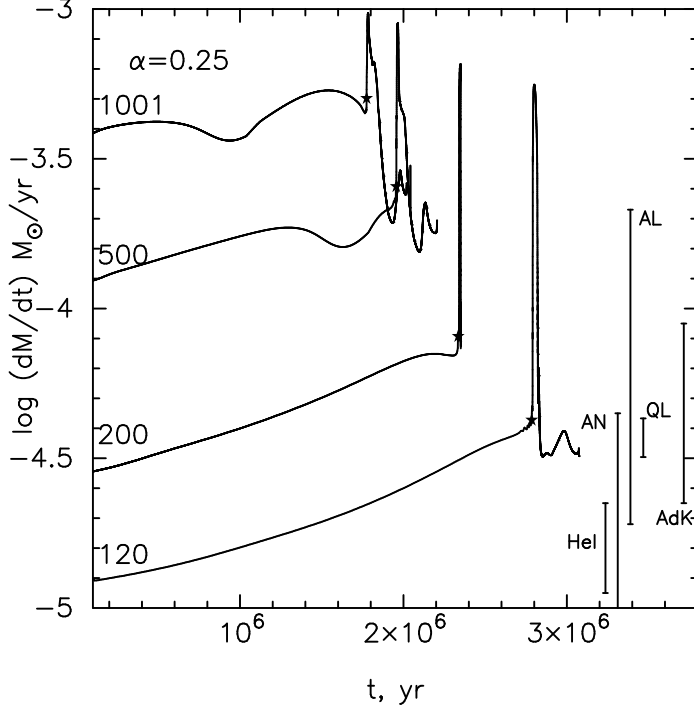
**Fig. 3.** Evolutionary tracks of stars in the Hertzsprung-Russel diagram. For 60  $M_\odot$ , the track for  $\alpha=0.25$  is shown; for 120  $M_\odot$ , tracks for  $\alpha=0.25$  and 0.5 are shown; for 200, 500 and 1001  $M_\odot$ , tracks for  $\alpha=0.25, 0.5, 0.8, 0.9$  and 1.0 are shown. The dotted line to the left shows the locus of homogeneous models. The dashed line indicates the Humphreys-Davidson limit (extrapolated for high  $T_{\text{eff}}$ ). The star symbol marks the position of a 133  $M_\odot$  star (indicating the bending point of the ZAMS). For orientation, the hatched rectangle shows the position of the Pistol star for the “low-luminosity” solution of Figer et al. (1998) and the diamonds show the position of  $\eta$  Car, which is somewhat uncertain because of the ambiguity in the radius determination (Hillier et al. 2001).



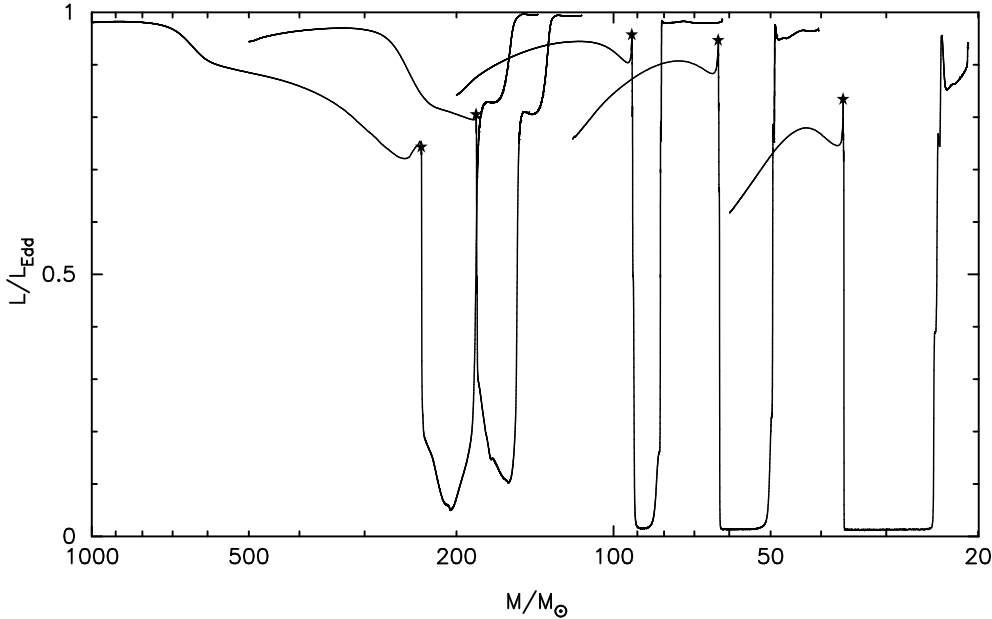
**Fig. 4.** Stellar mass vs. evolutionary lifetime for  $\alpha=1.0$ . Initial mass of stars is 1001, 843, 500, and  $200M_{\odot}$ . The dashed lines connect the loci of models with a hydrogen abundance in the convective cores of  $X_c = 0.6$  and  $0.5$ . The star symbols at the curves indicate the central hydrogen exhaustion time (see also Table 1).



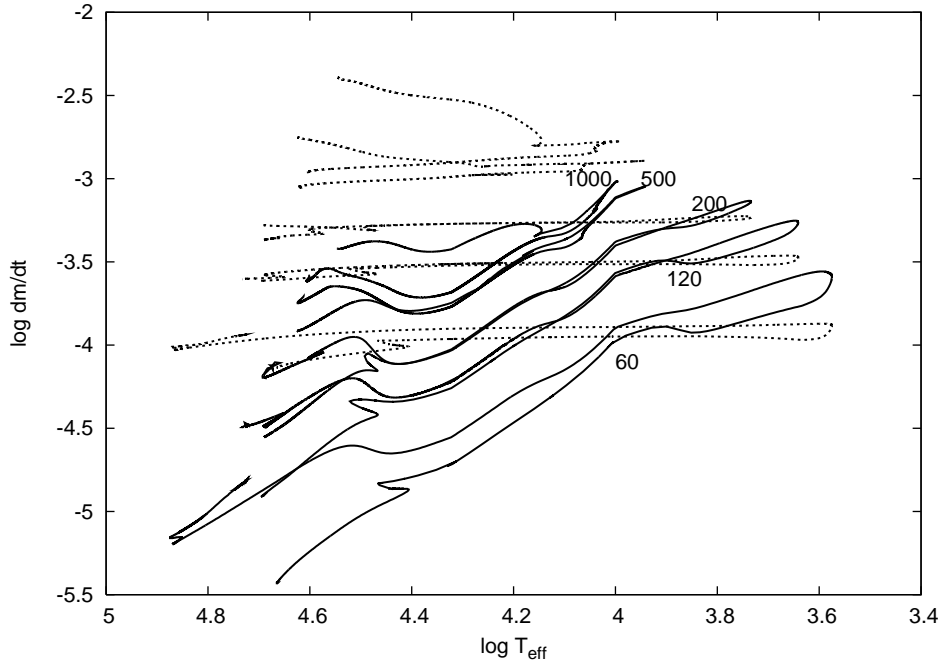
**Fig. 5.** Stellar mass vs. evolutionary lifetime for  $\alpha=0.25$ -sequences of stellar models. The dotted lines connect the loci of models with surface helium abundance 0.3, 0.4, 0.5, and 0.0. The dots at the curves indicate the time and mass when the hydrogen abundance in the convective cores  $X_c$  becomes 0.6(0.1)0.



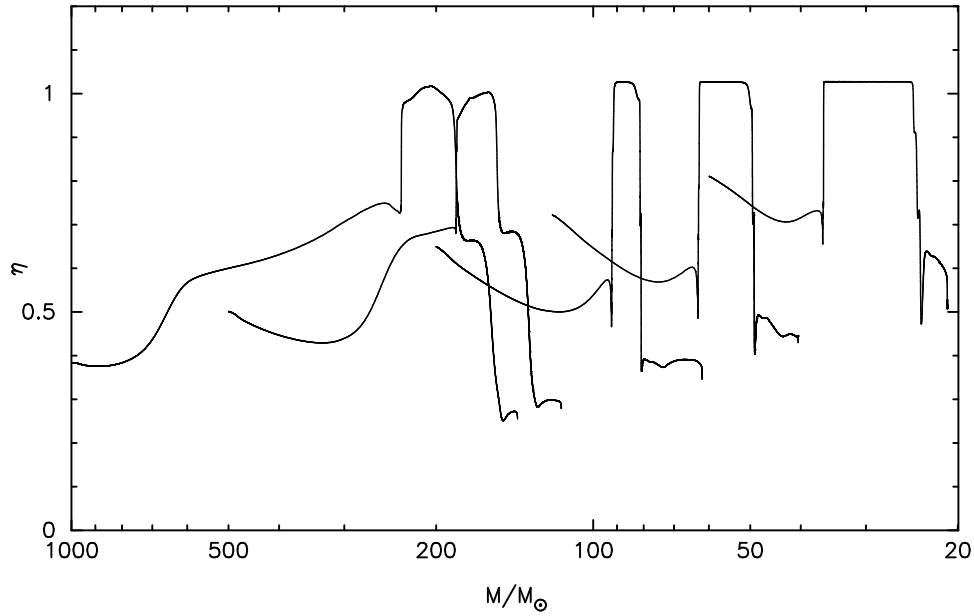
**Fig. 6.** Mass-loss rate vs. evolutionary lifetime for models with  $\alpha=0.25$ . The left border of the plots corresponds to  $t = 10^5$  yr, since mass-loss rates before this time are virtually the same as for the left extremes of the curves. The star symbols at the curves indicate the central hydrogen exhaustion time. Vertical bars show the ranges of the estimates of the mass-loss rate, obtained by means of quantitative spectroscopy for the Arches cluster (Najarro et al. 2004, AN), HeI emission stars in the Galactic center (Martins et al. 2007), star-forming-regions in the Galaxy and the Magellanic clouds (AdK, A.de Koter, unpublished), and estimates for the Arches and Quintuplet stars obtained by radio-observations (AL and QL, respectively, Lang et al. 2005). For the Quintuplet, only  $\dot{M}$  for stars identified with stellar winds are shown. In the Arches cluster, Lang et al. (2005) identify stellar winds for all observed sources.



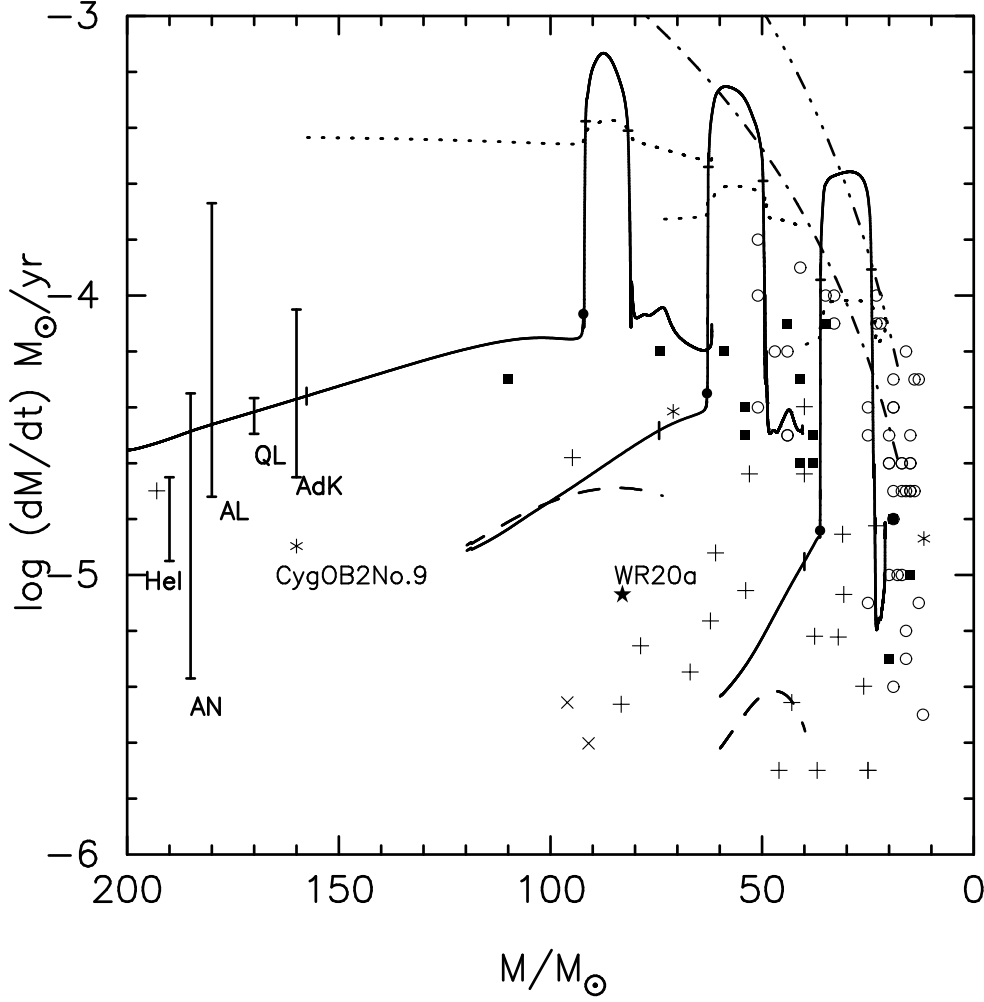
**Fig. 7.** The variation of  $L/L_{\text{Edd}}$  in the outer meshpoint of the models along evolutionary sequences for stars with  $M_0=1001, 500, 200, 120$ , and  $60 M_\odot$ , for  $\alpha=0.25$ . The star symbols label models with hydrogen abundance in the convective core  $X_c = 0$ .



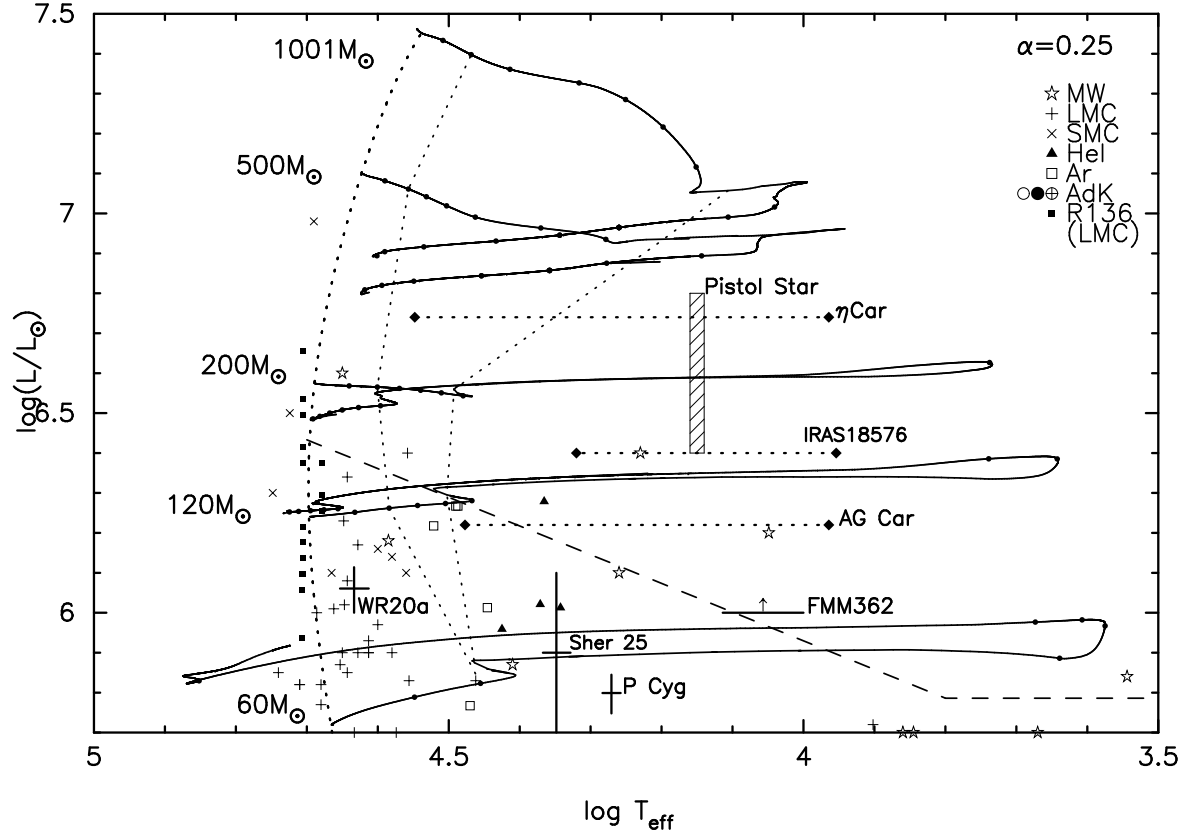
**Fig. 8.** The variation of the mass-loss rate versus  $T_{\text{eff}}$  for the  $\alpha=0.25$  sequence of stars (solid curves). For comparison, the dotted curves represent estimates of the maximum  $\dot{M}$  along the same tracks according to Eq. 6.



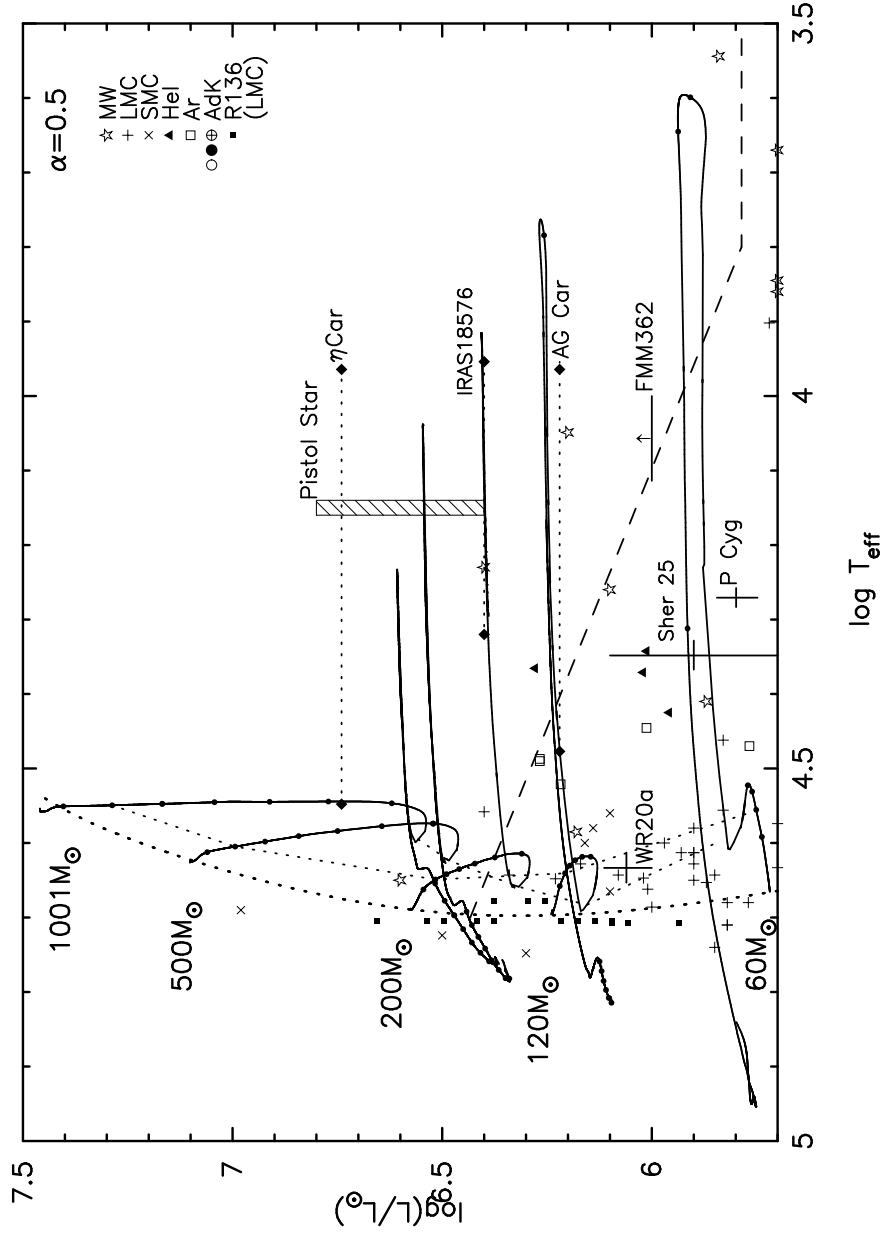
**Fig. 9.** The variation of the “wind performance number” along evolutionary tracks for  $\alpha=0.25$ .

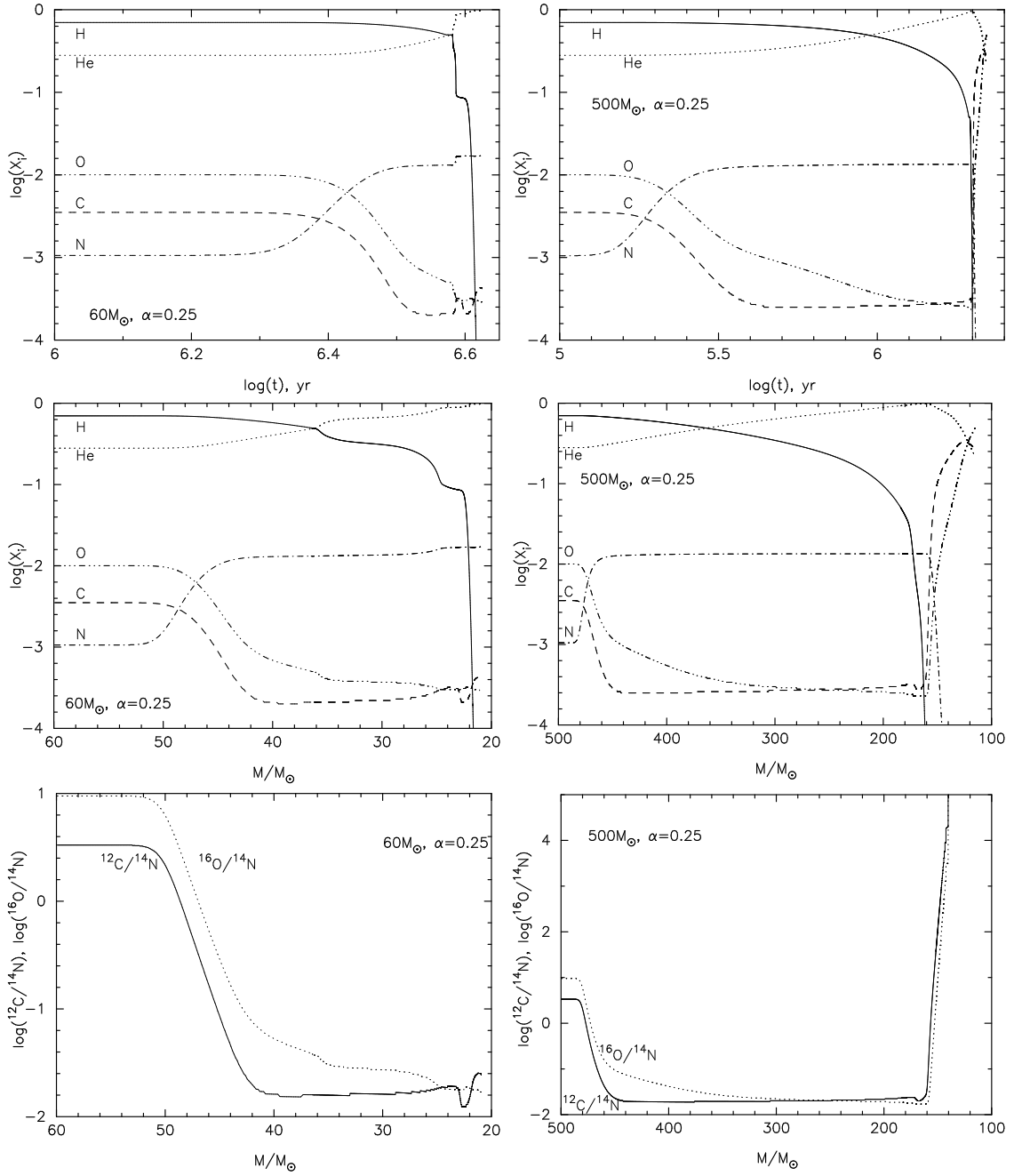


**Fig. 10.** The relation between stellar mass and mass-loss rate for the  $\alpha=0.25$  case. Ticks along the tracks (in the order of decreasing mass) indicate models in which the surface He-abundance becomes  $Y_s = 0.4$ , the last model with  $T_{\text{eff}} \geq 10000\text{ K}$  and  $Y_s \geq 0.4$ , and the first model in which  $T_{\text{eff}} \geq 10000\text{ K}$  again. The dots at the tracks mark the TAMS. The long-dashed line shows the mass-loss rate computed using the Vink et al. (2001) mass-loss formula. Dotted, dot-dashed, and dot-dot-dot-dashed lines show mass-loss rates for hydrogen-deficient WR stars from de Donder & Vanbeveren (2003), Langer (1989), and Nelemans & van den Heuvel (2001), respectively. Black squares represent estimates of stellar parameters of observed hydrogen-rich WR stars based on model atmospheres that account for iron-line blanketing and clumping (Hamann et al. 2006); open circles are estimates by the same authors for hydrogen-poor stars ( $X_H < 0.2$ ). Asterisks are spectroscopic mass and  $\dot{M}$  estimates for Galactic O-stars, plusses are estimates for LMC O-type stars, crosses are estimates for SMC stars (see Table 2 for references). The star symbol marks the position of the almost identical components of WR20a, currently the most massive star weighed in a binary system. Note its low  $\dot{M}$ . Vertical bars have the same meaning as in Fig. 6.



**Fig. 11.** Evolutionary tracks of stars in the Hertzsprung-Russell diagram (solid lines,  $\alpha=0.25$  case). Dots along the tracks show positions of models with surface helium abundance  $Y_s=0.3(0.1)0.9$ . Three dotted lines stretching from top to bottom connect ZAMS stars, the loci of models with surface He-abundance  $Y_c = 0.4$  (models with higher  $Y_c$  are conventionally considered as WR-stars), and TAMS stars. Broken long-dashed line shows the Humphreys-Davidson limit (linearly extrapolated at high  $L$  and  $T_{eff}$ ). The hatched rectangle shows the position of the Pistol star (see the text for comments). Also plotted are the positions of the most luminous stars in the Galaxy, the LMC, and the SMC (Table 2), the HeI-emission line stars in the Galactic center (Najarro et al. 1997), the Arches cluster stars (Najarro et al. 2004), luminous WNLh stars in the Galaxy and the Magellanic clouds (AdK, A. de Koter, unpublished) and the most luminous stars in the R136 cluster, with spectral subtypes O3 If\*, WN, O4If, and O3 III(f\*) (Massey & Hunter 1998, Table3). For AdK-stars, open circles are for the Galaxy, filled circles are for the SMC, crossed circles are for the LMC. See Appendix for the notes on particular stars.

Fig. 12. Same as Fig. 11 but for  $\alpha=0.5$ .





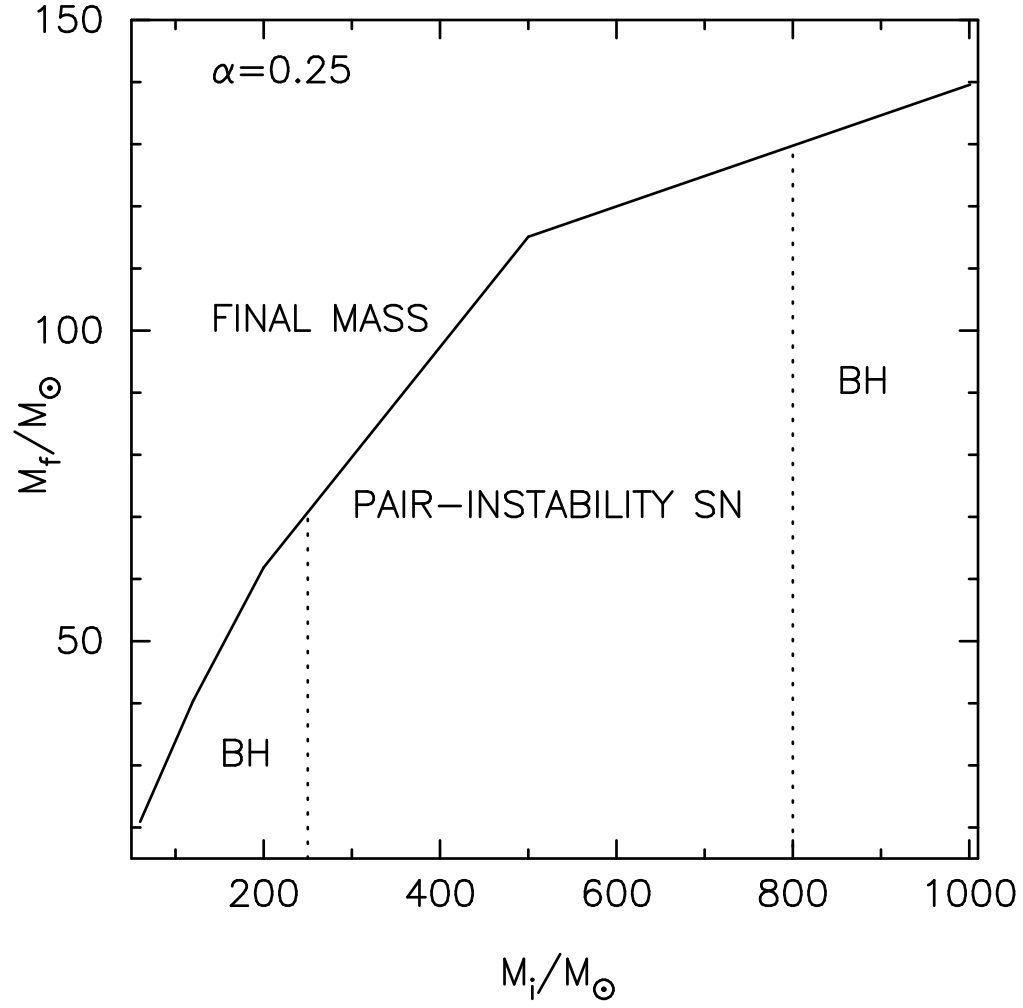


**Fig. 14.** Initial-final mass relation for SMS and inferred outcomes of evolution: black hole formation for progenitors with mass  $M_i \lesssim 250 M_\odot$  or  $M_i \gtrsim 800 M_\odot$ , and pair-instability supernovae in the intermediate range of  $M_i$ .

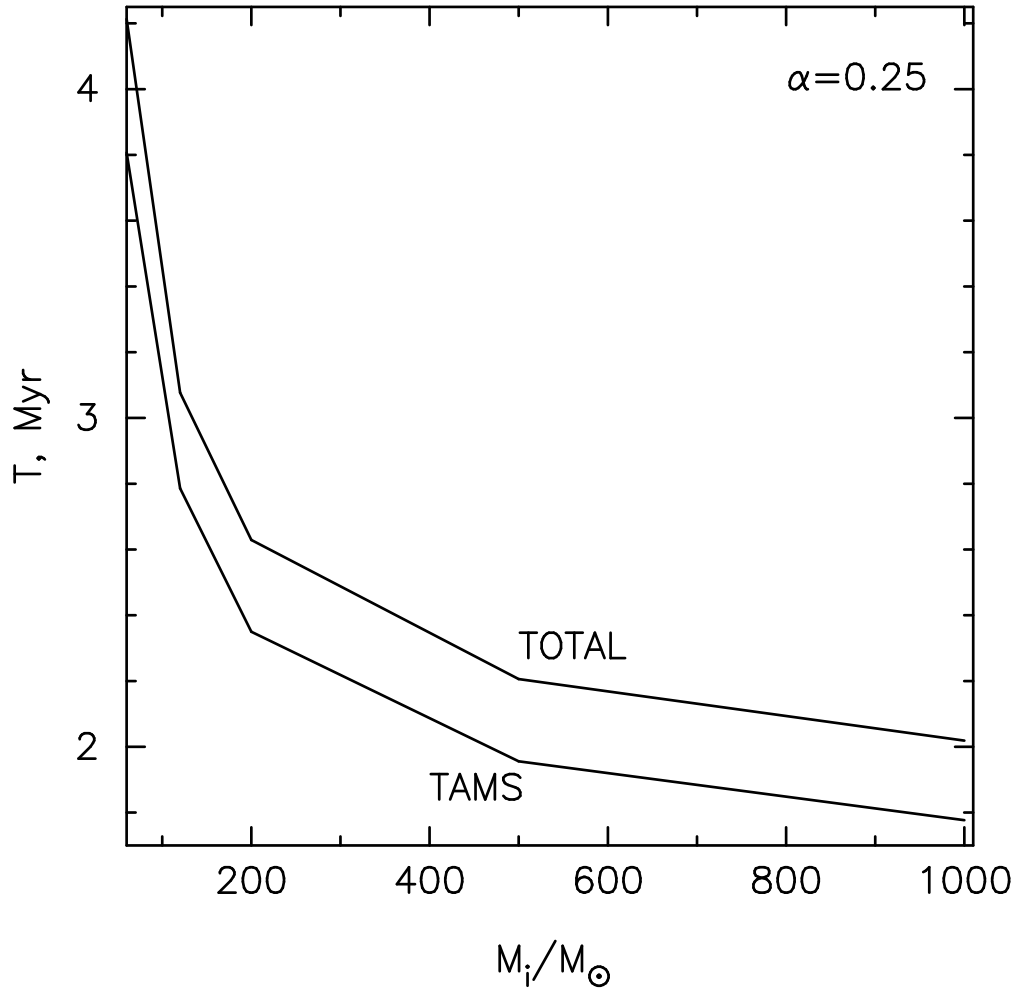


**Fig. 15.** Total lifetimes of supermassive stars and their lifetimes in the core-hydrogen burning stage.